

Review

An Insight into Carbon Nanomaterial-Based Photocatalytic Water Splitting for Green Hydrogen Production

Muhammad Asghar Rasool ¹, Rabia Sattar ¹, Ayesha Anum ², Sami A. Al-Hussain ³, Sajjad Ahmad ⁴, Ali Irfan ^{5,*} and Magdi E. A. Zaki ^{3,*}

¹ Department of Chemistry, The University of Lahore-Sargodha Campus, Sargodha 40100, Pakistan

² Hamdard Institute of Pharmaceutical Sciences, Islamabad Campus, Hamdard University of Pharmaceutical Sciences, Islamabad 44000, Pakistan

³ Department of Chemistry, College of Science, Imam Mohammad Ibn Saud Islamic University (IMSIU), Riyadh 13623, Saudi Arabia

⁴ Department of Chemistry, UET Lahore, Faisalabad Campus, Faisalabad 37630, Pakistan

⁵ Department of Chemistry, Government College University Faisalabad, Faisalabad 38000, Pakistan

* Correspondence: raialiirfan@gmail.com (A.I.); mezaki@imamu.edu.sa (M.E.A.Z.);

Tel.: +966-54-724-4888 (M.E.A.Z.)

Abstract: At present, the energy shortage and environmental pollution are the burning global issues. For centuries, fossil fuels have been used to meet worldwide energy demand. However, thousands of tons of greenhouse gases are released into the atmosphere when fossil fuels are burned, contributing to global warming. Therefore, green energy must replace fossil fuels, and hydrogen is a prime choice. Photocatalytic water splitting (PWS) under solar irradiation could address energy and environmental problems. In the past decade, solar photocatalysts have been used to manufacture sustainable fuels. Scientists are working to synthesize a reliable, affordable, and light-efficient photocatalyst. Developing efficient photocatalysts for water redox reactions in suspension is a key to solar energy conversion. Semiconductor nanoparticles can be used as photocatalysts to accelerate redox reactions to generate chemical fuel or electricity. Carbon materials are substantial photocatalysts for total WS under solar irradiation due to their high activity, high stability, low cost, easy production, and structural diversity. Carbon-based materials such as graphene, graphene oxide, graphitic carbon nitride, fullerenes, carbon nanotubes, and carbon quantum dots can be used as semiconductors, photosensitizers, cocatalysts, and support materials. This review comprehensively explains how carbon-based composite materials function as photocatalytic semiconductors for hydrogen production, the water-splitting mechanism, and the chemistry of redox reactions. Also, how heteroatom doping, defects and surface functionalities, etc., can influence the efficiency of carbon photocatalysts in H₂ production. The challenges faced in the PWS process and future prospects are briefly discussed.

Keywords: semiconductor; photocatalysis; water splitting; carbon nanomaterials; hydrogen production; solar irradiation



Citation: Rasool, M.A.; Sattar, R.; Anum, A.; Al-Hussain, S.A.; Ahmad, S.; Irfan, A.; Zaki, M.E.A. An Insight into Carbon Nanomaterial-Based Photocatalytic Water Splitting for Green Hydrogen Production. *Catalysts* **2023**, *13*, 66. <https://doi.org/10.3390/catal13010066>

Academic Editors: Amr Fouda and Mohammed F. Hamza

Received: 28 November 2022

Revised: 12 December 2022

Accepted: 15 December 2022

Published: 29 December 2022



Copyright: © 2022 by the authors. Licensee MDPI, Basel, Switzerland. This article is an open access article distributed under the terms and conditions of the Creative Commons Attribution (CC BY) license (<https://creativecommons.org/licenses/by/4.0/>).

1. Introduction

The global energy crisis and environmental challenges are crucial to producing clean, environmentally friendly energy. As pollution levels rise and the supply of fossil fuels declines, the market for green energy is escalating. Most of the world's power comes from fossil fuels, which pollute the atmosphere and contribute to global warming [1–3]. When fossil fuels are burned, 7.8 billion metric tons per year of CO₂ and other pollutants are released [4,5]. Fossil fuels account for practically all of the world's energy demands (86.4%) [6]. New energy sources can reduce or replace fossil fuels. Wind, hydroelectric, solar, geothermal, and other renewable energies are green and eco-friendly [7]. Solar energy can be used worldwide to generate electricity and heat. The Earth's atmosphere absorbs 3.85×10^{24} J of solar power annually. Currently, 2% of solar energy is converted into

green energy via various methods [8]. Photocatalytic materials are essential for converting solar energy directly into fuel [9]. Hydrogen generation as a future renewable, green fuel requires a quantum-efficient, stable photocatalyst [10]. Hydrogen has the potential to replace fossil fuels as an energy source. Water electrolysis requires voltages greater than 1.23 eV to produce hydrogen, owing to slow oxygen reactions [11]. Hydrogen is 2.75 times as energetic as hydrocarbon fuels and 2.40 times as active as methane. Hydrogen-powered fuel cells could produce both electricity and water. Scientists are using new methods and technologies with the defined requirements of green and cost-effective ways to create and store hydrogen energy. Introducing nanotechnology results in increased hydrogen generation and storage capacity [12]. Hydrogen can be produced through autothermal reforming, steam reforming, water electrolysis, and partial oxidation. Hydrogen generation systems include electrochemical, photochemical, and solar-assisted thermochemical systems [13]. In 1972, Fujishima and Honda devised a photocatalytic water-splitting (PWS) method using UV light for the first time. Since then, researchers have studied H₂ production using semiconductor photocatalysts [14]. Photocatalysis-based hydrogen production by direct water-splitting (WS) is an auspicious and renewable solution to the existing energy shortage [15]. The generation of hydrogen (H₂) and oxygen (O₂) can be accomplished by PWS when exposed to sunlight. Previous research on PWS focused on enhancing the photoactive material's effectiveness and durability [16]. Inorganic photocatalysts use light absorbers to generate electron-hole pairs, whereas cocatalysts reduce and oxidize water to create hydrogen and oxygen [17]. Metal-based photocatalysts are in high demand but are costly, corrosive, and potentially hazardous [18]. The MnO₂ nanosheet material is promising for electrochemical energy storage, electrocatalysis, and photocatalysis [19]. TiO₂ is the photocatalytic semiconductor that has received the most research over the past few decades. TiO₂-carbon composite displays significantly improved photocatalytic performance under solar irradiation [20]. TiO₂/MnO₂ nanocomposites have exceptional photocatalytic activity and solar energy consumption due to their small energy bandgap, negatively charged surface, and large specific surface area. Metal-based photocatalysts are being phased out in favor of other metal-free photocatalysts owing to their high band gap (~3.5 eV) [21,22]. Photocatalysts still face difficulties because of low quantum yield, excessive charge recombination, and limited light absorption [23]. To address the former requirements, one must look for inexpensive, broad-spectrum materials with effective internal charge transfer [22].

To improve photocatalysis, scientists are turning to carbon-based nanomaterials (CNMs) (Figure 1) such as graphene [24], carbon nanotubes (CNTs) [25], graphitic carbon nitride (g-C₃N₄) [26], fullerene (C₆₀) [27], carbon dots (CDs) [28], and carbon nanofibers (CNFs) [29], etc. Carbon-based nanomaterials show exceptional physicochemical properties, including thermal and chemical stability, high surface area, and better electrical, mechanical, and optical properties (Table 1). A variety of approaches are frequently used to fabricate CNMs such as arc discharge, chemical vapor deposition (CVD), laser ablation, and ball-milling [30]. Carbon nanomaterials have small band gaps, unique morphologies, and controlled structures. Low-dimensional materials are attractive possibilities for photocatalyst development [9]. Though CNMs own very little intrinsic photocatalytic activity, they can improve the efficiency of the active site of the photocatalyst as a carrier. Combining CNMs with a photocatalyst can improve the reagent's active center's adsorption site. Carbon-based nanomaterials with electron-hole pairs can also serve as electron acceptors or transmission channels to limit photoexcitation. Photocatalysts benefit from their ability to reduce particle aggregation and enhance particle distribution. The photothermal effects or photosensitivity of CNMs can be enhanced in the presence of light. Carbon-based nanomaterials can be a better option for PWS because they have many benefits, including low costs and a huge reserve. Researchers have extensively examined CNMs for H₂ production via light photocatalysis. Photocatalysts for H₂ production, such as carbon dots, are frequently employed. Progress has been made in CNM-photocatalyzed H₂ production.

This review describes the role of CNMs in the WS process for hydrogen synthesis in detail. The mechanism and redox reaction involved are also discussed. The study also

focuses on the factors that influence photocatalytic activity. The challenges and potential prospects of the PWS process are briefly discussed.

Table 1. Physical and chemical properties of CNMs.

Material	Young's Modulus	Thermal Conductivity (W/mk)	Tensile Strength	BandGap (eV)	Charge Career Mobility (cm ² /V·S)
Graphene	0.5–1.0 TPa	5000	130 GPa	0	2×10^5
Carbon Nanotubes	1–5 TPa	3500	13–53 GPa	1.1	1×10^5
Graphitic Carbon Nitride	210–320 GPa	3.5–7.6	25 GPa	2.7	-
Fullerenes	61–110 GPa	0.14–2.87	58–71 MPa	1.8	-
Carbon Quantum Dots	0.14–4.48 GPa	0.4	60–69 MPa	3.73	10^{-2} – 10^{-6}

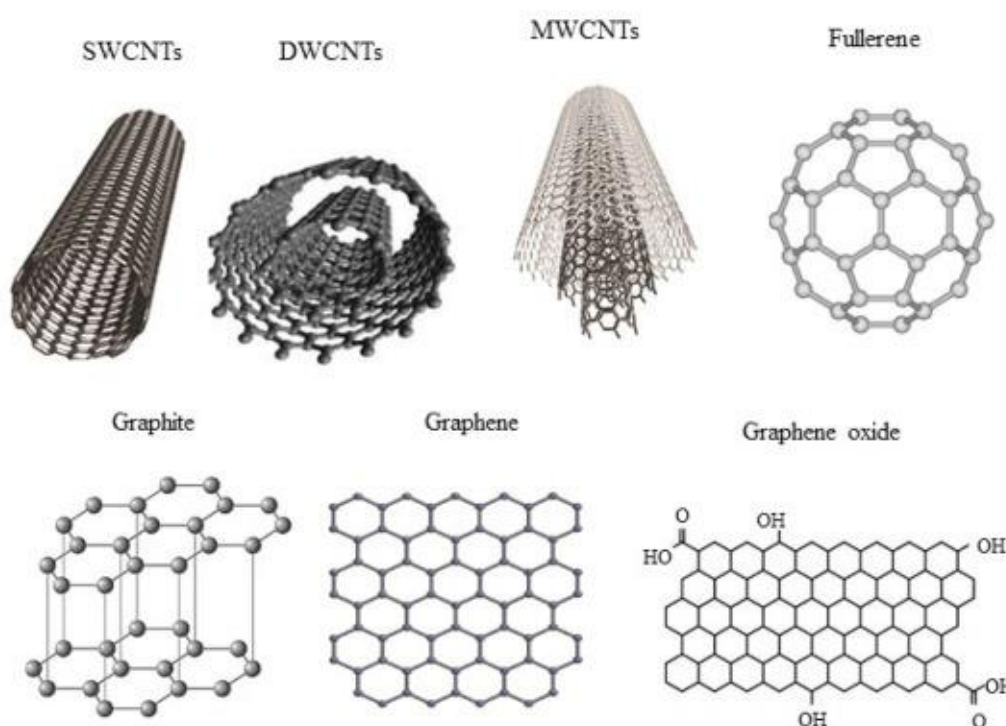
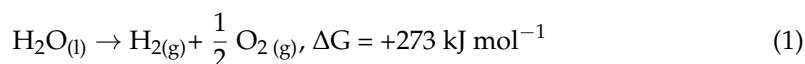


Figure 1. Structures of different Carbon-based nanomaterials. Reprinted/adapted with permission from Ref. [31]. Copyright © 2020, Elsevier.

2. Mechanism of Photocatalytic Water Splitting (PWS)

Fujishima and Honda were the first to decompose water using solar radiation successfully. TiO₂ and Pt can serve as anode and cathode electrodes in a photoelectrochemical cell. Under UV irradiation, this mechanism could divide water into hydrogen and oxygen [32]. A few years later, Bard applied the basic principles of this technology to develop the photocatalysis method. Since then, tremendous effort has gone into designing semiconductors that can dissolve water into H₂ and O₂ when exposed to light [33–36]. Photocatalysis begins with the photo-absorption of semiconductor photocatalysts. Under solar irradiation, holes are generated in the valence band VB that excite electrons to the conduction band CB. To interact with specific reagents, these charge carriers separate and move to the semiconductor surface [37,38]. For optimal photocatalytic activity, a semiconductor must have a bandgap bigger than 1.23 eV [39–41]. Then, the photo-excited electrons and holes must be quickly separated and migrated. On the photocatalyst surface, there must be a large number of adsorption sites and active centers [42]. A lower CB minimum than water's reduction potential (RP) is required for hydrogen evolution, while a higher VB maximum is required for oxygen evolution during photocatalysis [43–45]. Three significant steps involved in

photocatalysis are: (1) semiconductor photocatalysts absorb light to produce electron-hole pairs; (2) charge separation and surface migration in semiconductor photocatalysts; and (3) redox reaction happens for WS, electrons reduce water molecules to H₂, and holes oxidize them to O₂ [46–48]. The separation of hydrogen and oxygen from water is an endothermic process. Gibbs's free energy change for WS is +273.2 kJ mol⁻¹, according to Equation (3), equivalent to 1.23 eV per moved electron [39,49].



In semiconducting material, the conduction band CB must be more negative than the H⁺/H₂ redox potential. In contrast, the valence band VB of the semiconducting material must be more positive than the electrode potential of O₂/H₂O, i.e., 1.23 eV [39], as shown in Figure 2.

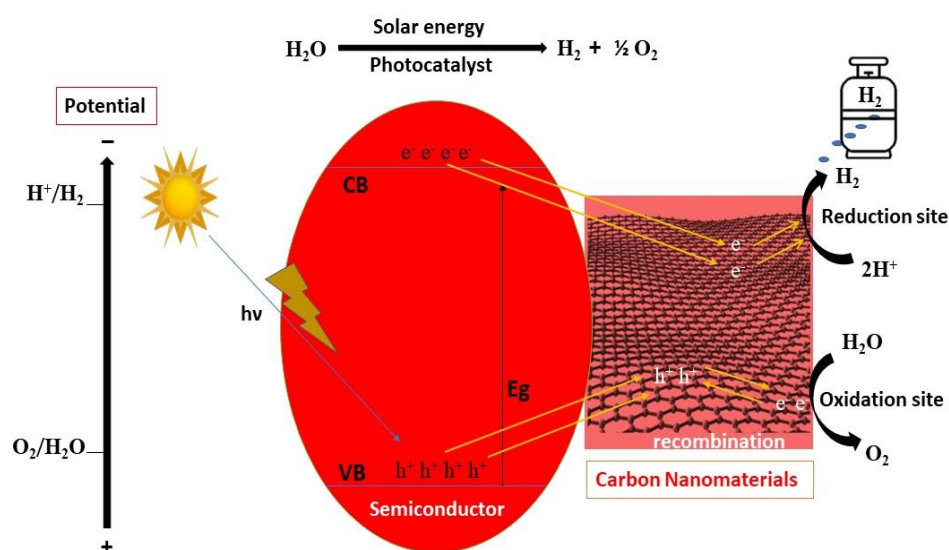


Figure 2. Photocatalytic water-splitting (PWS) mechanism.

However, unintentional electron-hole recombination is an essential concern in this method, substantially lowering photocatalytic efficacy [50–52]. The separation of electrons from holes can be improved by using CNMs to speed up carrier transit. Because of their high conductivity, CNMs can capture electrons driven by light in the CB of loaded semiconductors. When it comes to working function, CNMs perform significantly better than load semiconductors [40,53,54]. As a result, electrons are either trapped on the CNM's surface or are promptly transferred to the active site via the CNM's conductive surface [55]. Carbon nanomaterials display excellent semiconductor properties, including GO, rGO, CNTs, CDs, g-C₃N₄, and C₆₀. Developing a Schottky barrier between the metal catalyst and the CNMs semiconductor facilitates electron-hole pair separation during the deposition of the metal catalyst [56–59]. The difference in Fermi level between metal catalysts and CNMs semiconductors promotes charge flow until Fermi equilibrium, band bending, and Schottky barriers. Schottky barrier creation can efficiently restrict photogenerated electron backflow, permitting more electrons to contribute to hydrogen evaluation reaction (HER).

DFT calculations help better to understand photocatalytic HER on CNMs at the molecular and atomic levels. DFT's primary objective is to explore the active sites/defects available on the surface of CNMs. For example, among different types of CNMs, graphene might have a lot of edges or defects at its active site. The heteroatom interfaces with different materials and replaces the carbon atom [60]. The H₂ production mechanism can be described through theoretical construction and computational analysis. DFT investigations focus on the calculations related to electron density, structure elucidation, charge distribution, and energy of reaction [61].

3. Functions of CNMs in Photocatalytic H₂ Generation

3.1. Structural Support to Improve Structure Sustainability

In semiconductor photocatalysis, different carbon compounds such as CNTs, CDs, graphene, GO, and activated carbon (AC) serve as structural support [62–66]. Carbon nanomaterials offer a larger surface site for the dissemination and immobilization of nanoparticles (NPs). These inert and thermally stable CNMs maintain their structure and properties when coupled with NPs. Numerous defect and active sites (oxygen-based functional groups) present in carbon materials can be exploited to initiate the development and anchoring of homogenous nanoparticles. The carbon materials' light weight is essential for their use as structural support. It is now also possible to produce activated carbon, carbon fibers, CNTs, and graphene on a considerable scale and inexpensively due to the copious amount of carbon in the earth's crust. The presence of these carbon components can change nucleation and growth rates, slowing down semiconductor nanoparticle aggregation and strengthening their architectures [67–69]. This section discusses how carbon-based materials stabilize nanostructures. Thus, structural stability applies to component geometries and morphologies. Extremely small nanoparticles, clusters, or other nanostructures that are dispersed and stabilized can substantially increase structural strength. As a result, semiconductor nanoparticles possess a large surface area, numerous surface defects, and a superior contact interface with carbon materials for increased charge transfer. Therefore, carbon-based hybrid semiconductor photocatalysts are more effective at producing H₂ than pure semiconductor photocatalysts. The surface chemistry of carbon materials is greatly impacted by interactions between semiconductor nanoparticles and carbon material. Wang et al. [64] proposed that hydroxyl, carboxyl, carbonyl, and epoxy groups increased the hydrophilic property of the CNTs surface by first treating them with HCl and HNO₃. The Zn_xCd_{1-x}S nanoparticles were then supported by the functionalized CNTs using a solvothermal technique with the help of the raw ingredients including zinc acetate, cadmium chloride, and thiourea. The well-organized Zn_{0.83}Cd_{0.17}S nanoparticles on the CNTs surface have a diameter of about 100 nm. If CNTs were not there, these nanoparticles would stick together. The excellent dispersion improves the interfacial surface of the Zn_{0.83}Cd_{0.17}S/CNT photocatalyst. Since the conduction band of the photocatalytic material is more populated than the Fermi level of CNTs, photoexcited electrons will move to the surface of the nanotubes. Thus, the aforesaid phenomenon can efficiently separate photoinduced charge carriers at the photocatalyst's interface. In addition, CNT-incorporated Zn_{0.83}Cd_{0.17}S nanocomposite has a lower band gap value than pure Zn_{0.83}Cd_{0.17}S. Under 300 to 800 nm illumination, Zn_{0.83}Cd_{0.17}S/CNT nanocomposite generates 6.03 mmol·h⁻¹g⁻¹ of H₂, which is 1.5 times more than the pristine Zn_{0.83}Cd_{0.17}S.

Li et al. [70] prepared CdS-coupled graphene nanosheets via a hydrothermal approach using GO as supporting material, Cadmium acetate for Cd²⁺ precursor, and DMSO as the solvent as well as source of S²⁻. Solvothermal heating turned GO into graphene with CdS clusters on its surface. The interactions between nanoparticles and graphene can be strengthened by physical adsorption, the electrostatic force of attractions, and charge transference. The homogenous CdS cluster distribution on graphene, the CdS/graphene photocatalyst, has a greater specific surface area. Uniform CdS cluster distribution is attributed to the more effective transport of photoexcited charges to graphene. At 1.0 wt% graphene, 1.12 mmol·h⁻¹ of hydrogen is generated, which is 4.87 times than the neat CdS. Shen et al. [71] also used rGO additive to stabilize the very thin nanorods of Zn_{0.5}Cd_{0.5}S with a corresponding upsurge in photocatalytic H₂ evolution.

3.2. Cocatalyst

Cocatalysts in a photocatalytic system enhance H₂ evolution efficacy. Metals such as Pt, Au, or Pd have a more significant work function than semiconductors, making them excellent cocatalysts. Cocatalysts improve charge separation, provide catalytic sites, reduce over-potential, and minimize H₂ activation energy [72,73]. Noble metals are expensive and rare. Thus, economical cocatalysts are needed for economic photocatalytic systems. Carbon

compounds are effective cocatalysts for photocatalytic H₂ evolution [74,75]. The Fermi level of carbonaceous compounds is lesser than CB but RP is greater than H⁺/H₂. Carbon compounds have advantages similar to noble metal cocatalysts, with increased active sites and a localized photothermal effect owing to increased surface area and extended light absorption intensity [76,77]. Khan et al. [74] fabricated a CNTs/CdS/TiO₂/Pt photocatalyst via the hydrothermal method. Pt was designed onto TiO₂ via photodeposition whilst CdS via hydrolysis. This photocatalyst generates H₂ at a greater rate under visible radiations, using sodium sulfide and sulfate sacrificial agents. In the first step, the electrons and holes are separated between the TiO₂ and CdS interface. The photoelectron moves from the TiO₂ to the CNT surface and then Pt catalyst. The Pt nanoparticles work as cocatalysts due to their lower Fermi level of CNTs as compared to TiO₂. Both Pt and CNTs are promising photocatalysts and can improve the photo-catalytic H₂ evolution of CdS/TiO₂. Preferably, using 0.4 and 4 wt.% of Pt and CNTs, respectively, enhances the photocatalytic performance by 50%. A graphene/MoS₂/TiO₂(GMST) photocomposite was prepared hydrothermally using Na₂MoO₄, H₂NCSNH₂, and graphene oxide precursors at 210 °C and utilized as an efficient material for photocatalytic H₂ production [78]. It was exposed by using ethanol as a sacrificial agent and TiO₂ as the photocatalyst while graphene and MoS₂ functioned as cocatalysts. The GMST photocatalyst exhibited a high rate (~165.3 mol·h⁻¹) of H₂ generation at 5.0 and 0.5 wt.% of graphene and MoS₂, respectively, having 9.7% quantum efficiency (QE) at 365 nm [78]. A hybrid rGO/Zn_xCd_{1-x}S photocatalyst prepared first via coprecipitation and then a hydrothermal reduction approach elevates the cocatalytic performance for H₂ production [79]. A high rate of H₂ evolution (~1824 mol·h⁻¹g⁻¹) was observed for this optimized photocatalyst using 0.25 wt.% of rGO, which has 23.4% apparent QE at 420 nm under solar irradiation. Liu et al. integrated NH₃-treated CDs into g-C₃N₄ by heating CDs and urea for 3 h at 550 °C, where the carbon dots were first synthesized electrochemically and then hydrothermally treated with ammonia. This g-C₃N₄/CDs hybrid photocatalyst was found to be efficient in WS under solar light for the evolution of H₂ and O₂. A maximum QE of 16% was achieved using a g-C₃N₄/CD catalyst at 420 ± 20 nm. Actually, the photocatalytic action of g-C₃N₄ at the first stage caused water to be split into H₂O₂ and H₂, then, at the subsequent stage, the carbon dot-catalyzed breakdown of H₂O₂ into H₂O and O₂.

3.3. Photosensitization

Carbon compounds with semiconducting or dye-like characteristics can function as a photosensitizer in some cases, enhancing the photoresponse of a broad bandgap of the semiconductor photocatalyst by inducing additional photogenerated electrons [80–82]. The emission of photoelectrons from the material can overlap with semiconductor absorption and are responsible for the transfer of the resonance energy from the carbon material to the coupled semiconductor. As the result, the LUMO of the carbon material becomes more negative in comparison to the coupled semiconductor's CB. Wang et al. [83] prepared a graphene/ZnS (G-ZS) photocatalyst via the hydrothermal method for photocatalytic H₂ evolution under visible light. A graphene-supported ZnS photocatalyst evaluated 7.42 mol·h⁻¹g⁻¹ hydrogen at 0.1 wt.% graphene, which was found to be 8 times that of the pristine ZnS. Since visible light cannot excite ZnS, the photoelectron most likely originates from graphene and migrates to the CB of ZnS [80]. The rGO/Pt/TiO₂ photocatalyst is an excellent photosensitizer and evaluates H₂ at a rate of 11.24 mmol·h⁻¹g⁻¹. Carbon dots are excellent candidates for use as photosensitizers in photocatalytic reactions due to their high photo-absorption and photoluminescence properties. For instance, Martindale et al. [84] fabricated a carbon dot (photosensitizer)-based Ni-bis- (diphosphine) (NiP) photocatalyst for H₂ generation under visible light. To produce this photocatalyst, 30 nmol of NiP and 2.2 nmol of CD are used in 0.1M EDTA solution with pH 6; a photocatalyst g-CQDs/NiP produces H₂ at 398 mol·h⁻¹g⁻¹. The apparent QE at 360 ± 10 nm was observed ~1.4%. Carbon dots can convert near-infrared photons for semiconductor photocatalysis due to their photoluminescence up-conversion property [82,85]. Hydrogenated TiO₂(H-TiO₂)-

based photocatalysts were prepared with carbon quantum dots (CQDs) under bath reflux. This photocatalyst is UV-visible-NIR compatible and showed remarkable photocatalytic H₂ production capability under the illumination of a 300 W Xe arc lamp. For this photocatalytic system, Pt was used as the cocatalyst and methanol as the sacrificial agent across a wide spectral range. The higher H₂ generation rate of 7.42 mmol·h⁻¹g⁻¹ was observed in comparison to H-TiO₂ nanobelts (6.01 mmol·h⁻¹g⁻¹) [85].

3.4. Photocatalyst

Carbon-based nanomaterials are effective photocatalysts for H₂ generation, according to theory and experiment [86–88], owing to the semiconducting properties of CDs, CNTs, graphene, GO, rGO, and C₆₀. Such a nanocarbon of the semiconductor sort can have a greater number of negatively charged LUMO sites than H⁺/H₂ RP. Reduced graphene oxide rGO is a commonly used photocatalyst [89,90], as its CB minimum consists of anti-bonding π* orbital; at pH = 0, it has a potential of −0.52 eV [40]. Density functional theory (DFT) studies explain the electronic structure of graphene oxide by alternating the relative ratio of -OH and epoxy groups present on the surface. The resulting electronic structure shows the photocatalytic hydrogen, and oxygen evolution reaction occurs [91]. Teng's group reported that GO synthesized by a modified Hummers' method had an apparent direct E_g value of 3.3–4.3 eV and an indirect E_g of 2.4–3.0 eV. Graphene oxide (GO) is comprised of graphene molecules of different oxidation states and can produce H₂ under UV/Visible illuminations. In a 20% methanol aqueous solution with 0.5g GO and no cocatalyst, mercury lamp irradiation yielded 17,000 mmol·h⁻¹ H₂ [88]. Meng et al. [90] prepared a p-MoS₂/n-rGO photocatalyst with p-type MoS₂ deposited on the surface of n-type rGO. Under solar irradiation and ethanol as sacrificial agents, this photocatalyst exhibited higher H₂ evolution activity than bare MoS₂ and MoS₂/rGO. This is because, as shown by the photoelectrochemical experiment, the p-MoS₂/n-rGO junctions are very good at separating charges. Zhu's team compared H₂ production activity for neat CDs and CD-based composite materials [87,92,93]. An H₂ evolution at a 423.7 mol·h⁻¹g⁻¹ was achieved using carbon dots in pure water without needing a cocatalyst. Carbon dots were created hydrothermally from MWCNTs oxide [87]. In methanol sacrificial agent and Pt cocatalyst, a hybrid carbon nanodot/WO₃ photocatalyst produces H₂ at 1330 mol·h⁻¹g⁻¹ under xenon lamp irradiation [92].

3.5. Band Gap Narrowing Effect

Chemical bonds can form when semiconductor photocatalysts and carbon compounds make strong contacts (e.g., metal O C bonds). Chemical bonding reduces photocatalyst band gaps, increasing H₂ production [94,95]. Ye et al. [96] reported the hydrothermal fabrication of graphene/CdS (0.01:1) and CNTs/CdS (0.05:1) hybrid materials with the photocatalytic H₂ evolution of 52 mol·h⁻¹, respectively. The addition of graphene or CNTs into CdS resulted in the narrowing of the E_g values of these hybrid photocatalysts and consequently led to superior photocatalytic H₂ generation as compared to pristine CdS. This was in addition to the benefit of more effective charge separation. Bi₂WO₆ is often not used for water-splitting H₂ generation, due to its smaller RP and comparatively less negative CB. However, coupling Bi₂WO₆ nanosheets with graphene, the CB of Bi₂WO₆ becomes more negative, and the feasibility of photocatalytic H₂ evolution increases [97]. In a typical experiment [98], Bi₂WO₆ nanoparticles were produced via sonication onto the graphene's sheets using GO, HNO₃, (NH₄)₁₀W₁₂O₄₁, and Bi(NO₃)₃·5H₂O, followed by calcination at 450°C for 3h in an inert environment. Raman and XPS research validated the chemistry between Bi₂WO₆ and graphene. After coupling with graphene, Mott–Schottky calculations showed that the RP of CB of Bi₂WO₆ increased from +0.09 V to −0.30 V as compared to the standard hydrogen electrode. As a result, 0.03 g of Bi₂WO₆/graphene photocatalyst was used to produce 159.2 mol·h⁻¹ of H₂ at 420 nm in an aqueous solution of methanol.

In conclusion, in several aspects, carbon materials can significantly enhance the H₂ reaction rate compared to semiconductor photocatalysts. The inclusion of various carbonaceous materials coupled with semiconductor photocatalysts can result in a variety of proficient effects including structural support for improved structure constancy, electron collection, the reduction of the recombination rate of photo-stimulated charge pairs, photocatalyst, E_g narrowing outcome cocatalyst, and photosensitization. It is essential to remember that certain carbon materials can potentially play many functions throughout the entire photocatalytic process. Moreover, due to some limitations imposed by its structure and properties, a particular type of carbon material might not be able to fulfill all the functions. The potential characteristics of various CNMs are summarized in Table 2.

Table 2. Role of carbon nanomaterials in photocatalysis.

Function Type	Carbon Nanotubes	Graphene	Fullerenes	Graphene Oxide	Graphitic Carbon Nitride	Carbon Quantum Dots
Supporting material	✓	✓	×	✓	✓	✓
Photocatalyst	✓	✓	✓	✓	×	✓
Cocatalyst	✓	✓	✓	✓	✓	✓
Photosensitizer	×	✓	✓	✓	✓	✓
Bandgap narrowing effect	✓	✓	×	✓	✓	✓

4. Carbon-Based Nanomaterials for Photocatalytic H₂ Evaluation

4.1. Graphene-Based Composite Materials

Graphene is an allotropic form of carbon composed of monoatomic thick layers organized in a honeycomb pattern [99,100]. Its exceptional thermos-mechanical, electrical, catalytic, and optical features led to its use in different practical potentials [101]. Graphene is a potential candidate for photocatalysis applications owing to its large surface area and exceptionally high electron transference capability [102]. Graphene can be prepared differently, but frequently used methods include chemical vapor deposition (CVD), chemical and electrochemical exfoliation, and graphene oxide reduction [103,104]. Graphene oxide is an essential derivative of graphene with electrical and electronic properties. A pure graphite crystal structure must be oxidized to produce graphene oxide [105]. Graphene oxide sheets have several oxygenated functional groups on their surface which display distinct features from those of pristine graphene [106]. In addition, the average production cost of GO is less than that of G and numerous other nanomaterials. According to some studies and reports, the self-agglomeration of individual graphene-based photocatalysts prevents them from ever reaching their full potential in terms of efficiency [107].

Incorporating other nanomaterials into graphene layers is a promising technique to improve graphene layer exfoliation and characteristics [108]. These extraordinary features are particularly advantageous for fabricating photocatalytic nanocomposites based on graphene. Graphene-based hybrid nanocomposites have been identified as an essential material for O₂ and H₂ evaluation reactions [109]. The first principal calculations comprehensively explain the mechanism of PWS. The process begins with photoexcited electrons entering the graphene's LUMO and transporting the surface via π^* orbitals, resulting in the most significant possible charge separation. Carbon materials are excellent electron acceptors and transit channels for limiting photoinduced electron-hole pairs and improving the photocatalytic H₂ reaction rate [110].

Metal-doped graphene materials possess excellent photocatalytic capabilities due to maximum charge separation between VB and CB. TiO₂ is the most researched photocatalytic material on account of its thermodynamically stability, high oxidizing power, cost-effectiveness, and comparatively low toxicity [111]. The two most common phases of TiO₂ are rutile and anatase, with the E_g values of 3.2 and 3.0 eV, respectively. The UV light irradiation at wavelengths lower than 380 nm, which makes up around 1/20th of the entire solar spectrum on the Earth's surface, can only excite TiO₂ [112]. The integration of TiO₂ photocatalysts onto graphene is drawing interest. It offers the chance to address

all three methods of photocatalytic development simultaneously: enhanced contaminant adsorptivity, simple charge transit separation, and expanded light absorption range [113]. A G/TiO₂ composite photocatalyst with 5% graphene produced by the hydrothermal method, upon irradiation with UV-visible light without a cocatalyst, generates hydrogen at 86 mmol·h⁻¹g⁻¹ [114]. Nitrogen-doped graphene N/G is getting more attention because its physical, chemical, biological, and material science properties are much better than those of pure graphene [115]. Chemical vapor deposition is the most frequently used technique for the fabrication of N/doped graphene. In the CVD method, N and graphene precursors are utilized, and ammonia is a widely used source for N precursors [116,117]. When a neodymium-doped yttrium aluminum garnet (ND-YAG) laser shines on nitrogen-doped graphene in a methanol sacrificial agent, hydrogen produces at 6 mmol·h⁻¹. The photocatalytic efficiency of a nitrogen-doped semiconductor is increased because it has both n- and p-type conductivities [118,119]. Cu₂O is a promising photocatalyst because it is cheap, non-toxic, and has a narrow 2.2 eV band gap. Still, the photogenerated electrons and holes in Cu₂O are easily recombined, which is a critical issue regarding redox reaction progress. Graphene/Cu₂O hybrid material prepared by the CVD method also displays excellent semiconducting properties and evaluates hydrogen efficiently [120]. Cu₂O/doped graphene composite produces hydrogen at a rate of 19.5 mmol·h⁻¹ under visible light without needing a cocatalyst or sacrificial agent [121]. Park et al. synthesized Pt-TiO₂, GO-TiO₂, and a ternary hybrid of GO with Pt and TiO₂ for PWS hydrogen generation under UV irradiation. Also, they found that the combination of GO and Pt on TiO₂ could improve the H₂ activity, while GO acted as a cocatalyst [122]. Xiang et al. employed microwave-assisted hydrothermal treatment to develop TiO₂ nanosheets modified by GO, and the prepared hybrid material demonstrated improved photocatalytic H₂ generation in the presence of methanol (sacrificial agent). Surprisingly, in the absence of the Pt cocatalyst, the H₂ generation rate climbs 736 mmol·h⁻¹g⁻¹ with 3.1% quantum efficiency, exhibiting 41 times more performance than individual TiO₂ nanosheets [123]. The hydrogen efficiency of a binary and ternary hybrid composite (TiO₂/rGO, TiO₂/Pt, and TiO₂/rGO/Pt) is evaluated based on the charge-carrying capacity of reduced graphene oxide (rGO) and the efficiency of platinum nanoparticles as electron traps for photogenerated electrons. Compared to bare TiO₂, adding rGO to TiO₂ practically doubles the hydrogen generation rate (1.95%), and the TiO₂/Pt photocatalytic system performed best, with a 15.26 factor increase in hydrogen production compared to TiO₂ [124]. Specific to these materials is their ability to efficiently absorb visible light, due to their narrow bandgap and CB edge being more negative as compared to the RP of hydrogen positive ions. Pure CdS particles, on the other hand, still have several issues limiting their ability to produce H₂ [125,126]. Using a solvothermal process to synthesize graphene/CdS clusters, cadmium disulfide can be spread out well, making the photocatalyst's surface area bigger. Hydrogen was evolved at a rate of 70 mol·h⁻¹ using a xenon lamp irradiation source, graphene as a cocatalyst, and 0.1 M and 0.05 M of Na₂S and Na₂SO₃, respectively, as sacrificial agents [96]. Another important n-type semiconductor photocatalyst, Bismuth tungstate (Bi₂WO₆) with a narrow E_g of 2.69 eV, could have ability for absorbing photons from visible light. It has been much used as a photocatalyst to break down organic pollutants [127,128]. Because of its lower CB value, Bi₂WO₆ is an auspicious candidate for hydrogen generation from WS. When Bi₂WO₆ and graphene are combined by the electrodeposition method, the latter's CB shifts to a more negative state, which positions the former as the superior photocatalyst. Under the influence of ultraviolet light, hydrogen can be produced photocatalytically in the presence of methanol at a rate of 159.2 μmol·h⁻¹ [98]. In recent times, MoS₂ has gained widespread interest as an effective cocatalyst for the hydrogen evolution process. A nanocomposite of rGO/CdS was prepared via the solvothermal approach, employing DMSO as a reducing agent and S²⁻ source as well [70]. (NH₄)₂MoS₄ was used as a precursor of MoS₂, and was selectively photo-deposited on the surface of rGO by changing the pH of the solution. There have been no previous studies on the controlled photo-deposition of MoS₂ on the photocatalyst's surface for H₂ generation [69]. For PWS, a graphene/MoS₂/TiO₂

hydrothermally produced composite is employed. The effectiveness of the combined photocatalytic process is improved by the use of both graphene and MoS₂. With a xenon arc lamp, graphene/MoS₂/TiO₂ generates hydrogen at a rate of 165.3 $\mu\text{mol}\cdot\text{h}^{-1}\text{g}^{-1}$ in aqueous methanol [78]. GO/ZnCl₂/Na₂S demonstrates photocatalytic efficiency that is eight times greater compared to pristine GO. Without a sacrificial agent, this combination generates hydrogen having a rate of 7.42 $\text{mol}\cdot\text{h}^{-1}$ when exposed to visible light [83].

Zn_xCd_{1-x}S is a phenomenal material with photosensitive and photocatalytic properties. The heterojunction of graphene with Zn_{0.8}Cd_{0.2}S synthesized by the co-precipitation hydrothermal process displays photocatalytic hydrogen production [129]. Under the influence of solar irradiation, it can produce hydrogen at a rate of ~1824 $\mu\text{mol}\cdot\text{h}^{-1}$ without any cocatalyst, while sodium sulfide and sulfates are provided as sacrificial agents [78]. Ternary photocatalysts (NiS/Zn_xCd_{1-x}S/rGO) are synthesized having enhanced photocatalytic H₂ production efficacy under simulated solar radiation. One of its key features is this photocatalyst's co-loading of NiS and rGO on NiS/Zn_xCd_{1-x}S. rGO can provide an active reduction site for synthesizing H₂ and behave as an electron accumulator and transporter. NiS can assemble photoexcited holes between NiS and Zn_xCd_{1-x}S nanostructures because of nanoscale p-n junctions. Photogenerated electrons and holes are easily separated, leading to strong photocatalytic H₂ generation. Without a cocatalyst and sacrificial agent, an rGO/NiS/Zn_{0.5}Cd_{0.5}S photocatalyst synthesized via the co-precipitation method and hydrothermal treatment generates hydrogen at 375.5 $\text{mol}\cdot\text{h}^{-1}$ [130]. Lin et al. synthesized a ternary photocatalyst UiO-66/CdS/rGO by photodeposition, with a 13.8 times higher photocatalytic hydrogen production rate compared to pure CdS, and even demonstrated significant advantages over the commendably ideal composite material P25/CdS/rGO [131]. rGO was used to stabilize the ultra-thin Zn_{0.5}Cd_{0.5}S nanorods with an increased photocatalytic H₂ evolution of 1.12 $\text{mmol}\cdot\text{h}^{-1}$. Compared to pure CdS particles, this rate was 4.87 times higher. TiO₂ doped with 5 wt.% graphene exhibits a hydrogen production rate of 8.6 $\text{mmol}\cdot\text{h}^{-1}$, which is found to be 1.9 times more than the neat P25. The hydrogen evolution rate of 40.9 $\text{mmol}\cdot\text{h}^{-1}$ under visible illumination was observed for the ZnIn₂S₄ photocatalyst with 1 wt.% loading of rGO using lactic acid (sacrificial agent). However, pure ZnIn₂S₄ has the rate of only 9.5 $\text{mmol}\cdot\text{h}^{-1}$. With an ideal concentrations of rGO (0.25 wt.%) and NiS (3 mol%), the fabricated ternary hybrid photocatalyst displayed the maximum rate of H₂ production (375.7 $\text{mmol}\cdot\text{h}^{-1}$) [132,133]. A tabularized summary of graphene-based photocatalysts for H₂ production is given in Table 3.

Table 3. Graphene-based composites and H₂ evaluation rate.

Composite Material	Cocatalyst	Sacrificial Agent	Irradiation Source	Rate of H ₂ Production	Reference
TiO ₂ /doped graphene	graphene	0.1 M Na ₂ S and 0.04 M Na ₂ SO ₃	Visible light	86 $\text{mmol}\cdot\text{h}^{-1}\text{g}^{-1}$	[114]
N/doped graphene	None	Methanol	ND-YAG laser	6 $\text{mmol}\cdot\text{h}^{-1}\text{g}^{-1}$	[118]
Graphene/Cu ₂ O	None	None	Visible light	19.5 $\text{mmol}\cdot\text{h}^{-1}\text{g}^{-1}$	[121]
Graphene/CdS	graphene	Na ₂ S and Na ₂ SO ₃	Xenon lamp	70 $\mu\text{mol}\text{h}^{-1}\text{g}^{-1}$	[96]
G/Bi ₂ WO ₆	None	Methanol	Visible light	159.2 $\mu\text{mol}\text{h}^{-1}\text{g}^{-1}$	[98]
G/MoS ₂ /TiO ₂	MoS ₂	Ethanol	Xenon arc lamp	165.3 $\mu\text{mol}\text{h}^{-1}\text{g}^{-1}$	[78]
rGO/Zn _{0.8} Cd _{0.2} S	None	Na ₂ S and Na ₂ SO ₃	Solar irradiation	1824 $\mu\text{mol}\text{h}^{-1}\text{g}^{-1}$	[78]
GO/ZnCl ₂ /Na ₂ S	graphene	None	Visible light	7.42 $\mu\text{mol}\text{h}^{-1}\text{g}^{-1}$	[83]
rGO/NiS/Zn _{0.5} Cd _{0.5} S	None	None	Solar irradiation	375.5 $\mu\text{mol}\text{h}^{-1}\text{g}^{-1}$	[130]

4.2. Carbon Nanotubes (CNTs)

Iijima discovered carbon nanotubes for the first time in 1991 [134,135]. Among all the allotropes of carbon, the most promising and investigated allotropes are CNTs, exhibiting sp² hybridization. Few materials in nanotechnology are as unique as CNTs [136]. These are renowned for their electric conductivity and chemical stability and have been used as one of the most promising catalytic support materials [137–142]. Carbon nanotubes are classified

as either single-walled or multi-walled CNTs, based on the number of graphitic layers present [143,144]. Several methods for manufacturing carbon nanotubes have been devised, including arc discharge, CVD from hydrocarbons, and laser ablation, etc. Arc discharge is one of the primeval processes of synthesizing CNTs [145]. The arc discharge method uses the thermal dispersion of graphite electrodes in plasma. Chemical vapor deposition uses hydrocarbon gases to develop single- and multi-walled carbon nanotubes [146–148]. Carbon nanotubes are promising catalysis materials and can be used as catalysts, additives, or support. A number of metals and their oxides are found to be excellent catalysts [149,150] for the generation of hydrogen on the surface of CNTs, synthetic fuel [151], as well as the intermediates that are used in the production of polymers and artificial fibers [152–154]. Carbon nanotubes' poor dispersion in solvents results from their low chemical compatibility, exacerbated by their poor van der Waals interactions and hydrophobicity [155,156]. However, because of their vast functionalization capabilities, they are more soluble in a wide range of solvents [157].

Regarding photocatalysis, CNTs are attractive carbon semiconductors due to their unique electrical properties, such as high conductivity and electroluminescence, as well as their vast surface area and high tensile strength [158,159]. Coupling CNTs with other catalytic materials can improve their photocatalytic activity. The solvothermal decomposition of a single-source molecular precursor in the presence of ethylene glycol resulted in a CNTs/CdS composite [160]. CdS is an advanced semiconducting substance that, in its purest state, can evaluate hydrogen at a rate of $14.5 \mu\text{mol}\cdot\text{h}^{-1} \text{g}^{-1}$ with 0.1 M Na₂S and 0.05 M Na₂SO₃ used as a sacrificial agent under a xenon lamp. The CdS/CNTs composite material improves hydrogen photocatalytic activity and yields $52 \mu\text{mol h}^{-1} \text{g}^{-1}$ of hydrogen under identical conditions [96]. Iron oxide nanoparticles have excellent adsorption, biocompatibility, and electrocatalytic activity. Although iron oxide nanoparticles have several advantages, they are limited in electrochemical sensors due to poor dispersion and high levels of aggregation [161,162]. Multi-walled carbon nanotubes/iron oxide nanocomposites MWCNTs/Fe₂O₃ can be prepared by the in situ flame synthesis method and are an efficient photocatalyst for hydrogen synthesis [163]. The photoelectrochemical H₂ efficacy of MWCNTs/Fe₂O₃ nanocomposites is $85 \text{ L h}^{-1} \text{m}^{-2}$ [164]. TiO₂ absorbs only a little percentage of solar UV radiation and endures photogenerated charge carrier recombination. TiO₂ has been modified with carbonaceous materials (Figure 3), absorbing more solar energy and slowing down the electron-hole recombination process [165]. Compared to a pure TiO₂ semiconductor, the photocatalytic material consists of functionalized carbon nanotubes and titanium dioxide (TiO₂/FCNTs) prepared by the arc discharge method and shows significantly increased hydrogen production at a rate of $2134 \text{ mmol}\cdot\text{h}^{-1} \text{g}^{-1}$ under solar irradiation and glycerol as a sacrificial agent. [63,166].

Kang et al. reported the hydrothermal synthesis of the CuO/NiO photocatalyst with CNTs as a structural support. Herein, the CuO/NiO nanomaterial provides active reaction sites, Eosin Y acts as a sensitizer, and triethanolamine (TEOA) is utilized as a sacrifice reagent for photocatalytic H₂ evolution under visible light. A rate of H₂ evolution of $\sim 1.0 \text{ mmol}\cdot\text{h}^{-1} \text{g}^{-1}$ was achieved under optimum conditions [167]. Surface-functionalized carbon nanotube-cadmium sulfide SF/CNTs/CdS composites displayed higher photocatalytic H₂ production activities when exposed to solar irradiation than pure CdS nanorods ($2.5 \text{ mmol}\cdot\text{h}^{-1} \text{g}^{-1}$). The composite material SF/CNTs/CdS evaluates H₂ at a rate of $6.1 \text{ mmol}\cdot\text{h}^{-1} \text{g}^{-1}$, when platinum is utilized as a cocatalyst, and solar light is used as the radiation source [168]. Another phenomenal nano-semiconducting material, zinc ferrite ZnFe₂O₄ coupled with CNTs (CNTs/ZnFe₂O₄), produces hydrogen at $18 \text{ mmol}\cdot\text{h}^{-1} \text{g}^{-1}$ under a mercury lamp irradiation source using aqueous methanol sacrificial agent [169]. Compared to single and two-component systems, anisotropic ternary core-shell Zn_{0.5}Cd_{0.5}S/TiO₂/MWCNTs photocatalysts exhibit significantly higher photocatalytic activity. Under solar irradiation, composite material Zn_{0.5}Cd_{0.5}S/TiO₂/MWCNTs generates hydrogen at a rate of $21.9 \text{ mmol}\cdot\text{h}^{-1} \text{g}^{-1}$ without the need for a sacrificial agent or catalyst [170]. Alternatively, metal sulfide, ZnS was extensively considered for catalytic H₂

generation. However, its wide E_g restricts the light response in the visible range. To move this E_g into the visible region, more effort has been put into doping ZnS and creating solid solutions of $Cd_{1-x}Zn_xS$. Additionally, it has been demonstrated that sulfide solid solutions such as $Cd_{1-x}Zn_xS$ are effective photocatalysts for H_2 production from WS under visible range [171–173]. The CNTs/ $Cd_{0.1}Zn_{0.9}S$ photocatalyst is prepared by a simple hydrothermal method, and is an excellent material for H_2 evaluation in the visible spectrum [80]. As with the pure $Cd_{0.1}Zn_{0.9}S$ semiconductor, the CNTs/ $Cd_{0.1}Zn_{0.9}S$ composite evaluates hydrogen with a $78.2 \text{ mmol}\cdot\text{h}^{-1}\text{g}^{-1}$ rate of reaction in the absence of a cocatalyst and sacrificial agent [79]. A well-assembled layer of $Zn_{0.83}Cd_{0.17}S$ nanostructures with $\sim 100 \text{ nm}$ diameter was fabricated onto the CNT surface. The $Zn_{0.83}Cd_{0.17}S$ /CNTs photocatalyst has a higher interfacial area owing to the excellent dispersion of nanotubes. As the potential of the CB of $Zn_{0.83}Cd_{0.17}S$ is more negative as compared to the nanotubes' Fermi level, the photoexcited electrons will travel from this material to the surface of the CNTs. The benefit described above can thus effectively separate photo-stimulated charge transporters at the interface of nanotubes and $Zn_{0.83}Cd_{0.17}S$. The CNT-coupled nanocomposite's band gap was also tuned to a lower value when compared to neat $Zn_{0.83}Cd_{0.17}S$. H_2 was produced 1.5 times as quickly by the CNTs-incorporated nanocomposite with a photocatalytic rate of $\sim 6.03 \text{ mmol}\cdot\text{h}^{-1}\text{g}^{-1}$ [174]. A solvothermal technique was used to create a $Zn_{0.83}Cd_{0.17}S$ nanocomposite modified with carbon nanotubes. At the optimal amount (0.25 wt.%) of CNTs, the prepared $Zn_{0.83}Cd_{0.17}S$ /CNTs nanocomposites exhibit the maximum photocatalytic performance when exposed to a Xe lamp, with a $5.41 \text{ mmol}\cdot\text{h}^{-1}\text{g}^{-1}$ reaction rate [175]. Using irradiation ranging from 300 to 800 nm, the $Zn_{0.83}Cd_{0.17}S$ /CNTs nanocomposite produced 1.5 times as much H_2 per hour as pure $Zn_{0.83}Cd_{0.17}S$. The photocatalytic H_2 generation rate of the CNTs/ $Cd_{0.1}Zn_{0.9}S$ composite was $78.2 \text{ mmol}\cdot\text{h}^{-1}$ at 420 nm. Only $24.1 \text{ mmol}\cdot\text{h}^{-1}$ of pure $Cd_{0.1}Zn_{0.9}S$ was produced [176,177]. Also, a ternary photocatalyst Co coupled with N-doped CNTs was prepared by heating cobalt acetate and melamine together at $800 \text{ }^\circ\text{C}$. This composite material, Co/N-CNTs, produces H_2 at a $14.7 \text{ mmol}\cdot\text{h}^{-1}\text{g}^{-1}$ reaction rate [178]. A tabularized summary of CNT-based photocatalysts for H_2 generation is given in Table 4.

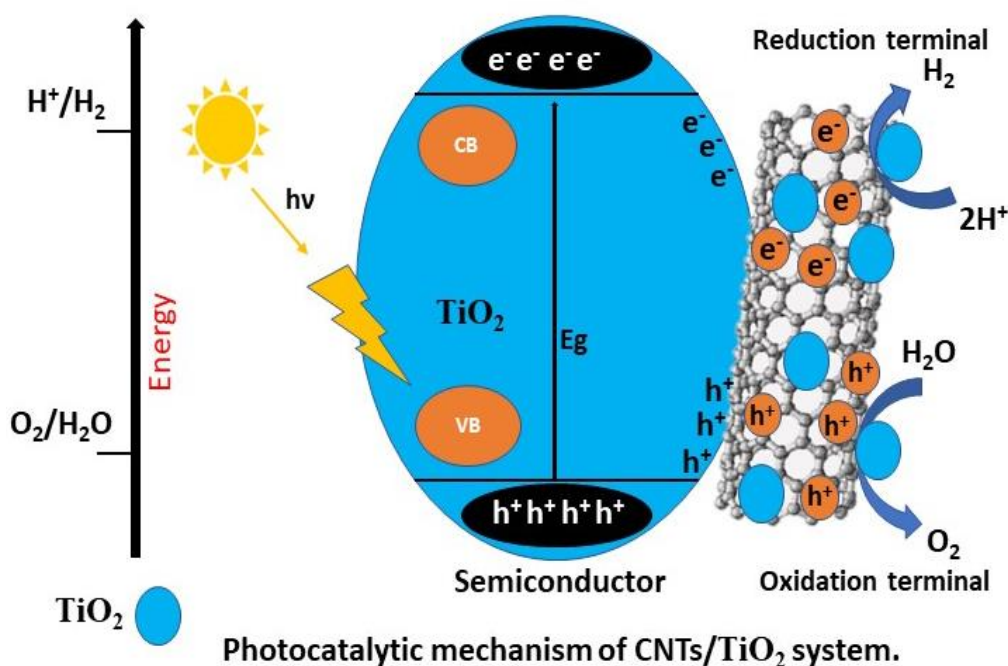


Figure 3. The CNTs/TiO₂ composite for hydrogen production.

Table 4. Rate of H₂ production by CNT-based photocatalysts.

Composite Material	Cocatalyst	Sacrificial Agent	Irradiation Source	Rate of H ₂ Production	Reference
CNTs/CdS	None	Na ₂ S and Na ₂ SO ₃	Xe lamp	52 μmol h ⁻¹ g ⁻¹	[96]
ZnO/CNTs	Pt	Water-methanol (1:4)	UV-visible	1 μmol h ⁻¹ g ⁻¹	[157]
TiO ₂ /FCNTs	None	Glycerol	Solar light	2134 mmol·h ⁻¹ g ⁻¹	[63]
CuO/NiO/CNTs	CuO/NiO	Triethanolamine	Visible	1 mmol·h ⁻¹ g ⁻¹	[167]
Ascorbic acid/CNTs/CdS	Pt	None	Sunlight	120.1 mmol·h ⁻¹ g ⁻¹	[168]
CNTs/ZnFe ₂ O ₄	None	Methanol	Mercury lamp	18 mmol·h ⁻¹ g ⁻¹	[169]
Zn _{0.5} Cd _{0.5} STiO ₂ /Multi-walled CNTs	None	None	Solar light	21.9 mmol·h ⁻¹ g ⁻¹	[179]
CNTs/Cd _{0.1} Zn _{0.9} S	None	None	None	78.2 μmol h ⁻¹ g ⁻¹	[79]
Co/NCNTs	None	None	Visible light	14.7 mmol·h ⁻¹ g ⁻¹	[178]
Zn _{0.83} Cd _{0.17} S/CNTs	None	S ²⁻ , SO ₃ ²⁻	UV-visible	6.03 mmol·h ⁻¹ g ⁻¹	[64]

4.3. Graphitic Carbon Nitride (g-C₃N₄)

Over the last decade, g-C₃N₄ has been intensively studied as a promising semiconductor. This material has mechanical properties similar to diamond due to its cyamelurine (C₆N₇)-consisted units and strong covalent interactions between C and N atoms. In addition, it is thermally, chemically, and photochemically stable too [180,181]. g-C₃N₄ is a conventional semiconducting material with an E_g value of 2.7 eV. Its semi-conductive properties are utilized in photocatalytic HER and CO₂ reduction reactions as well [182–184]. g-C₃N₄ is nontoxic and has a high level of biocompatibility, so it has minimal adverse environmental impacts [185] and can be cost-effectively fabricated on the massive scale [186]. It has various benefits for photocatalytic HER over other standard photocatalysts, including a strong light absorption capacity, greater surface area, exceptional superficial features, superior elemental stability, and cost effectiveness [187–190]. For the production of g-C₃N₄ heterojunctions, various procedures have been used due to the material's extraordinary structural stability. There are multiple methods to accomplish this, including ion exchange, electrodeposition, co-precipitation, electrospinning, and the high-temperature solid-phase process [191,192]. Some inexpensive and commonly used nitrogen precursors are urea, cyanamide, dicyandiamide, and melamine as building blocks in the thermal condensation process to make g-C₃N₄ [42,193,194]. However, the photocatalytic performance of g-C₃N₄ is less than other photocatalysts despite its use with different photocatalysts. The recombination rate of e⁻/h⁺ for g-C₃N₄ is very high, which limits its capacity to reduce H₂ [65]. It can absorb light only at 460 nm, limiting its ability to gather considerable amounts of radiation. The covalently bonded hydrogen over the surface of g-C₃N₄ is also accountable for the lowered rate of H₂ production in the 0.1–4.0 mmol·h⁻¹g⁻¹ range [159,195]. Hydrogen generation from aqueous environments, the photocatalytic reduction of CO₂ and other organic/inorganic pollutants, NO_x degradation, and the detection of O₂ activation sites have all relied heavily on g-C₃N₄ [196–201]. g-C₃N₄ as a comparatively innovative catalyst in the photocatalysis development process utilized to degrade water was firstly reported by Wang et al. [202,203]. However, in g-C₃N₄ there is an insufficient transference of photoexcited e⁻(s) and h⁺(s), and the strong recombination of e⁻/h⁺ pairs restricts the application of the photocatalyst [204,205]. It is possible to overcome it by the doping of the g-C₃N₄ structures with various metals and nonmetals [206,207] and heterojunction photocatalysts formed by associating with metal and semiconductor nanoparticles [208,209].

MoS₂/g-C₃N₄ composite heterojunctions are suitable candidates for photocatalytic H₂ evaluation reactions [210–212]. MoS₂ has recently become a popular photocatalyst and electrocatalyst because of its low bandgap, which matches the solar spectrum, and its ability to resist photo-corrosion. Therefore, MoS₂ is generally stated to be a semiconduc-

tor cocatalyst. Lu et al. used the ultrasonic agitation method to make g-C₃N₄/MoS₂ to avoid the contamination of organic pollutants such as methyl orange (MO), ciprofloxacin (CPFX), and tetracycline (TCY). Impregnating MoS₂ into mesoporous g-C₃N₄ resulted in a high-performance heterojunction for producing H₂ [213–215]. The effectiveness of TiO₂ as a photocatalyst has led many researchers to rely solely on it for their PWS experiments. Combining TiO₂ with another semiconductor material increases its efficiency by a factor of a hundred or more. The thermal condensation of the TiO₂/g-C₃N₄ nanocomposite with TEOA sacrificial agent produces 286 mmol·h⁻¹g⁻¹ of H₂ [216], whereas the hydrogen evaluation rate of pure g-C₃N₄ is 54.13 mmol·h⁻¹g⁻¹ [217]. Ag-loaded g-C₃N₄ has recently gained popularity as a photocatalyst in many fields. Ag quantum dots/g-C₃N₄ composite was fabricated via a one-step mix-calcination technique by Chen et al. for PWS. The maximum HER efficiency was increased by 4.6 times in comparison to g-C₃N₄ under a visible range [218]. Under visible light irradiation, Sun et al. used binary photocatalysts of Ag/g-C₃N₄ nanostructures to remove NO_x from the air [219]. Graphene has gained significant consideration in nanomaterials for its distinct electronic characteristics, greater surface area, and elastic structure. The electronic structure of g-C₃N₄ can be efficiently altered by the flawless in-plane combination of g-C₃N₄ and graphene via continuous π conjugation interactions, where graphene's exceptional electron capability contributes to unconstrained in-plane e⁻/h⁺ segregation and transference [220,221]. G/g-C₃N₄ composite evaluates hydrogen at 0.451 mmol·h⁻¹g⁻¹ [222]. Rh has been extensively studied as an active component for water hydrolysis among metals. It is widely known as a catalyst support and significantly impacts the catalytic activity of supported metal nanoparticles (NPs). Here, g-C₃N₄ was made easily and in large amounts by burning urea in the air. The resultant material was used to help stabilize Rh-NPs so they could be used to turn water into hydrogen. The g-C₃N₄/Rh nanocomposite produces hydrogen at 60 μ mol h⁻¹g⁻¹ [17]. Metal-free catalysts can be retained by doping semiconductors with nonmetal impurities, which can then be used to improve their photocatalytic properties by altering the semiconductors' electronic structures and morphology [223]. In the periodic table, boron, carbon, and nitrogen all share the same atomic size, making it possible to introduce B atoms into the framework of g-C₃N₄ [224]. Boron-doped g-C₃N₄ nanosheets can be synthesized using microwave heating, a fast and green method [225]. The B/g-C₃N₄ composite generates hydrogen at 94 μ mol·h⁻¹g⁻¹ without cocatalyst and sacrificial agent [226]. Carbon nanostructures that have been doped with N atoms have been found to have improved electron transfer and a wider range of visible light adsorption properties [227,228]. The nitrogen-doped graphitic carbon nitride N/g-C₃N₄ photocatalyst prepared by the hydrothermal method displays enhanced photocatalytic hydrogen production at 44.28 μ mol h⁻¹g⁻¹ [3].

Hydrogen was produced more efficiently in photocatalytic systems using nickel compounds such as nickel oxide [229], nickel sulfides [230], nickel phosphide [231], and nickel pyrophosphate [232], all of which were loaded onto carbon nitride as photocatalysts for the decomposition of water [233]. A photocatalyst synthesized by the thermal polymerization of amorphous nickel pyrophosphate (a-Ni₂P₂O₇) supported onto the g-C₃N₄ generates hydrogen at 207 μ mol h⁻¹g⁻¹ [232]. Tungsten oxide WO₃ has received much attention because it absorbs visible light, is chemically stable, and moves electrons well [234]. In recent years, WO₃ has been used in many different areas, such as photocatalysts [235], gas sensors [236], electrochromic displays [237], etc. The VB and CB positions of g-C₃N₄ are higher as compared to neat WO₃, so their band structures are similar [238]. A hydrothermally produced tungsten oxide composite with g-C₃N₄WO₃/g-C₃N₄ has a high H₂ evaluation capacity of 963 mmol·h⁻¹g⁻¹ in the existence of TEOA sacrificial agent [239]. In the same way, WO₃/g-C₃N₄/Ni(OH)_x, made in two steps (calcination and photodeposition) using TEOA as a sacrificial agent, can produce 576 mmol·h⁻¹g⁻¹ of hydrogen [240]. Cheng et al. produced 400 mmol·h⁻¹g⁻¹ of H₂ by thermally treating WO₃/g-C₃N₄ nanomaterial with TEOA sacrificial agent [241]. A HER of 1853 mmol·h⁻¹g⁻¹ was achieved using the same graphitic carbon-nitride heterojunction with tungsten oxide after adjusting the synthesis conditions [242]. Under visible light irradiation, the optimal heterostructures of

g-N₃N₄ with 10wt. % loadings of nanodiamonds (NDs) exhibit HER of 59.1 mmol·h⁻¹ [243]. The boron-doped carbon nanodiamonds with g-C₃N₄ heterojunction (B/CNDs/g-C₃N₄) have an optimum HER and apparent QE of 96.3 mmol·h⁻¹ and 6.91%, respectively, at 420 nm, which is approximately 5 and 2 times greater than the pure g-C₃N₄ nanosheets, 18.2 mmol·h⁻¹ and 3.92%, respectively [244]. Furthermore, loading 8 percent Ni₃C@Ni NPs with a nickel shell-layer thickness of 15 nm on g-C₃N₄ resulted in the maximum HER of 11.28 μmol h⁻¹ compared to the binary g-C₃N₄/Pt nanostructure. A higher HER over g-C₃N₄ proved that Ni₃C@Ni mounted a more effective cocatalyst than the well-known noble metal Pt [245]. A tabularized summary of g-C₃N₄-based photocatalysts for H₂ generation is given in Table 5.

Table 5. H₂ production rate with reported g-C₃N₄-based photocatalysts.

Composite Material	Morphology	Synthesis Method	Sacrificial Agent	H ₂ Activity	Reference
g-C ₃ N ₄	Nanoparticles	Chemical exfoliation	Triethanolamine	54.13 mmol·h ⁻¹ g ⁻¹	[217]
N/g-C ₃ N ₄	Nanoparticles	Hydrothermal method	Triethanolamine	44.28 mmol·h ⁻¹ g ⁻¹	[3]
TiO ₂ /g-C ₃ N ₄	Nanoparticles	Thermal condensation	Triethanolamine	286. mmol·h ⁻¹ g ⁻¹	[216]
G/g-C ₃ N ₄	Nanoparticles	-	Methanol	0.451 mmol·h ⁻¹ g ⁻¹	[222]
Rh/g-C ₃ N ₄	Nanoparticles	-	Methanol	60 mmol·h ⁻¹ g ⁻¹	[17]
B/g-C ₃ N ₄	Nanoparticles	-	Triethanolamine	94 mmol·h ⁻¹ g ⁻¹	[226]
g-C ₃ N ₄ /a-Ni ₂ P ₂ O ₇)	Nanoparticles	Solvothermal method	Triethanolamine	207 mmol·h ⁻¹ g ⁻¹	[232]
WO ₃ /g-C ₃ N ₄	Nanoparticles	Hydrothermal, calcination	Triethanolamine	963 mmol·h ⁻¹ g ⁻¹	[239]
WO ₃ /g-C ₃ N ₄ /Ni(OH) _x	Nanoparticles	Calcination, photodeposition	Triethanolamine	576 mmol·h ⁻¹ g ⁻¹	[240]
WO ₃ /g-C ₃ N ₄	Nanoparticles	One-pot preparation	Triethanolamine	400 mmol·h ⁻¹ g ⁻¹	[241]
WO ₃ /g-C ₃ N ₄	Nanoparticles	Post-thermal treatment	Triethanolamine	1853 mmol·h ⁻¹ g ⁻¹	[242]
g-C ₃ N ₄ /WO ₃ /BCS	Nanoparticles	One-pot heat method	20 vol% Triethanolamine	2500 mmol·h ⁻¹ g ⁻¹	[246]

4.4. Fullerenes (C₆₀)

Buckminsterfullerene C₆₀, discovered in 1985, is considered the most representative zero-dimensional carbon substance. Fullerenes are CNMs with varying structural forms (hollow sphere, ellipsoid, etc.) [247]. Fullerenes are good building blocks for supramolecular assemblies and functional micro- and nanostructures due to their well-defined structures, high electron-receiving ability, and electron-transport capacity. The orderly structure of fullerene molecules can potentially affect or improve fullerene micro/nanostructure (FMNSs) properties [248–250]. Various techniques, such as arc discharge, laser ablation, chemical vapor deposition (CVD), the laser irradiation of polyaromatic hydrocarbons (PAHs), and the resistive arc heating of graphite, can all be utilized in the synthesis of fullerenes. In the beginning, fullerene was produced by laser-vaporizing carbon in an atmosphere devoid of oxygen, but this method only produced a small amount of the material [31,251]. For the large-scale production of fullerene C₆₀, an electrical arc is used to heat graphite while a laser irradiates polycyclic aromatic hydrocarbons. A supersonic expansion nozzle and a pulsed laser can be used to create fullerene on graphene (G) coupled with helium gas. Carbon is vaporized off a spinning graphite sheet using a focused pulsed laser and transferred to a high-density helium stream. Fullerenes and their derivatives are used in organic photovoltaics [252], antioxidants [253], biopharmaceuticals [31], polymer additives [254], catalysts [255], water purification protection catalysts [256], portable power devices [257], and automotive components [258]. In addition, they are ideal for storing medical and gas supplies. Many advantages come with fullerenes. However, their dispersion and solubility in solution are poor. Fullerene derivatives' photocatalytic characteristics

have been extensively explored as a result. Bai et al. created a photocatalyst to remove organic dyes by replacing the fullerene with a hydroxyl group, which was then combined with titanium dioxide [259]. In recent years, scientists have found encouraging results from fullerene-based composite nano-photocatalytic materials in removing organic contaminants, photocatalytic hydrogen synthesis, photovoltaic cells, photocatalytic organic synthesis, and sterilization [259–263]. Several fullerene/semiconductors have been developed for photocatalytic wastewater treatment and WS, including C_{60}/TiO_2 , C_{60}/ZnO , C_{60}/CdS , $C_{60}/g-C_3N_4$, and others. Fullerene/semiconductor photocatalysts can be produced using various synthetic techniques, such as simple adsorption, hydrothermal/solvothermal synthesis, the sol-gel method, and mechanical ball-milling [264]. Chai et al. synthesized a $TiO_2/C_{60}/dCNTs$ photocatalyst, and when it was exposed to UV light, it was found to improve photocatalytic H_2 production. It produced H_2 at a rate of 651 mol h^{-1} using 5 wt% loading of C_{60} . That is 2.9 times as much as bare TiO_2 [54]. Regarding dye degradation and H_2 production, Tahir et al. have recently stated that the WO_3/C_{60} nanocomposite has a greater photocatalytic efficiency [265]. Shahzad et al. synthesized a WO_3 /fullerene photocatalyst using a simple photodeposition method using 1.5% $Ni_3B/Ni(OH)_2$ as a cocatalyst for H_2 production. The photocatalytic efficiency of $WO_3/C_{60}/Ni_3B/Ni(OH)_2$ in H_2 generation was exceptional, reaching $1578 \text{ mol h}^{-1} \text{ g}^{-1}$ [266]. Song et al. produced a range of C_{60} -modified Fe_2O_3 polymorph photocatalysts utilizing a simple adsorption technique. These as-prepared samples displayed enhanced photocatalytic efficiency for H_2 production at $0.3218 \text{ mmol}\cdot\text{h}^{-1} \text{ g}^{-1}$ under xenon lamp irradiation [267].

Although Cr_2O_3 nanoparticles are stable and cheap, the 3.4 eV bandgap value limits their applications in H_2 production [268,269]. The high surface area of fullerene also provides more photocatalytic sites for the photocatalysts. This way, a metallic oxide modified with C_{60} could be an ideal system for improving photoinduced electron migration efficiency. $Cr_{2-x}Fe_xO_3$ -type photocatalysts are synthesized using a simple absorbing process and used in photocatalytic hydrogen evolution. The photocatalytic H_2 evolution rate of $0.2205 \text{ mmol}\cdot\text{h}^{-1} \text{ g}^{-1}$ is significantly enhanced in the as-prepared $C_{60}/Cr_{2-x}Fe_xO_3$ nanocomposites in the presence of a TEOA sacrificial agent under xenon lamp irradiation [270]. A tabularized summary of fullerene-based photocatalysts for H_2 production is given in Table 6.

Table 6. Fullerene-based materials and H_2 production rate.

Photocatalyst	Function of NMs	Light Source	Sacrificial Agent	H_2 Production Rate	Reference
C_{60}/MoS_2	Photosensitizer	Xenon lamp	Triethanolamine	$6.89 \text{ mmol}\cdot\text{h}^{-1} \text{ g}^{-1}$	[262]
$WO_3/C_{60}/Ni_3B/Ni(OH)_2$	None	None	None	$1578 \text{ mol h}^{-1} \text{ g}^{-1}$	[266]
C_{60}/Fe_2O_3	Photosensitizer	Xenon lamp	Triethanolamine	$0.3218 \text{ mmol}\cdot\text{h}^{-1} \text{ g}^{-1}$	[267]
$C_{60}/Cr_{2-x}/Fe_xO_3$	Photosensitizer	Xenon lamp	Triethanolamine	$0.2205 \text{ mmol}\cdot\text{h}^{-1} \text{ g}^{-1}$	[270]
C_{60}/CdS	Photosensitizer	Xenon lamp	10 vol% lactic acid and 1wt%Pt	$1.73 \text{ mmol}\cdot\text{h}^{-1} \text{ g}^{-1}$	[271]
C_{60}/TiO_2	Photosensitizer	Xenon lamp	Triethanolamine	$0.5792 \text{ mmol}\cdot\text{h}^{-1} \text{ g}^{-1}$	[272]
$C_{60}/\text{graphene}/g-C_3N_4$	Photosensitizer	LED irradiation	Triethanolamine	$0.0946 \text{ mmol}\cdot\text{h}^{-1} \text{ g}^{-1}$	[273]

4.5. Carbon Quantum Dots (CQDs)

Carbon quantum dots are a novel and economical type of quasi-spherical nanocarbon particle with a diameter of less than 10 nm [274–276]. Carbon quantum dots, a fluorescent nanomaterial class, have recently received much attention due to their distinct optical and photodegradation features compared to organic dyes [277,278]. Researchers are looking into how CQDs can be used as catalysts. Much research and development have gone into making fluorescent nanoparticles that are non-hazardous. Top-down and bottom-up methods are used to synthesize CQDs. Top-down methods include laser ablation, arc discharge, electrochemical and plasma therapy. Examples of bottom-up techniques include pyrolysis, microwave-assisted, chemical oxidation, reverse micelle, and others. Carbon quantum dots

(CQDs) are efficient photosensitizers that produce hydrogen in an aqueous solution using solar radiation [84]. Carbon quantum dots exhibited photocatalytic activity in the visible region beyond >455 nm and maintained their overall photocatalytic activity for at least one day under full solar spectrum illumination. There is no evidence to support using CQDs for photocatalytic methods that are not constrained by cost, toxicity, or scalability issues [279]. Carbon quantum dots can be used in numerous photocatalytic processes with their high specific surface area and electron storage capacity. Carbon quantum dots in photocatalysis can create more active reaction sites by improving light absorption across a more comprehensive wavelength range [45,280,281]. Carbon quantum dot/semiconductor composites formed predominantly by physical adsorption were used to study the photocatalytic degradation of organic dye pollutants in the liquid or gas phase when exposed to visible and infrared light. It is critical to the photocatalytic activity of these composites that the CQDs in these composites have a conjugated structure [282,283]. Composites containing copper and CQD were more efficient at releasing H_2 than pure copper nitrate (Cu-NPs). The maximum rate of H_2 evolution for a sample containing 15.6 wt% CQDs was $64 \text{ mmol}\cdot\text{h}^{-1}\text{g}^{-1}$ [284]. There has been research into the photodegradation of MB by nanocomposite TiO_2 -CQDs. An enhanced photocatalytic activity is achieved by increasing electron energy in the TiO_2 -CQDs nanocomposite under illumination by a xenon lamp [285]. That is the first report of a novel and auspicious photocatalyst based on the surface plasmon resonance (SPR) of Ag NPs and the conversion property of CQDs to enhance the broad range of light absorption and photogenerated charge transference of $g\text{-}C_3N_4$ in photo-driven HER [276]. Yang et al. created $g\text{-}C_3N_4$ heterostructures (CCTs) by polymerizing freeze-dried urea and CQD precursor at high temperatures. During the co-condensation process, they discovered that implanted CQDs might actively induce tube assembly. That results in creating micro-regional heterostructures, facilitating the passage of photoelectron carriers. The photovoltaic properties of the CCTs were excellent compared to the photoelectrochemical properties of pure $g\text{-}C_3N_4$ and CQD-adsorbed $g\text{-}C_3N_4$ (CQD/ $g\text{-}C_3N_4$) nanosheets [286]. Yu et al. described a new CQDs/ $ZnFe_2O_4$ composite photocatalyst produced through a modest hydrothermal process initially. The CQDs/ $ZnFe_2O_4$ (15 vol %) composite exhibits an approximately 8-fold more significant transient photocurrent response than $ZnFe_2O_4$; this shows that electron-hole pairs generated by photosynthetic processes have higher transfer and separation efficiencies [287]. For the formation of H_2 , Zhu's group studied both pure CDs and composite photocatalysts based on carbon dots. Pure CDs, made hydrothermally from MWCNTs, photocatalyzed the pure water with HER of $423.7 \text{ mmol}\cdot\text{h}^{-1}\text{g}^{-1}$ in the absence of any cocatalyst. The Z-scheme carbon nanodots/ WO_3 hybrid photocatalyst produced H_2 at a rate of $1330 \text{ mmol}\cdot\text{h}^{-1}\text{g}^{-1}$ under xenon lamp illumination, with methanol serving as a sacrificial agent and Pt serving as the cocatalyst [87,92,93]. Yu et al. reported the preparation of CQD-modified P25- TiO_2 composites (CQDs/P25) via the one-step hydrothermal method. The CQDs/P25 showed superior photocatalytic H_2 evolution than the pure P25 without use of any other noble metal cocatalyst under UV-Vis and visible light irradiation ($\lambda > 450$ nm) [281]. The photocatalytic material 5% CDs/ $NiCo_2O_4$ was created hydrothermally and then calcined. This composite photocatalytic material utilized uniformly loaded CDs to decrease the recombination of photoexcited charges and accelerate the photoinduced electron transference. In the CDs/ $NiCo_2O_4$ composite (CDs, 5%), the optimum HER at normal atmospheric pressure is $62 \mu\text{mol}\cdot\text{h}^{-1}\text{g}^{-1}$ and OER is $29 \mu\text{mol}\cdot\text{h}^{-1}\text{g}^{-1}$, which is approximately four times greater than the pristine $NiCo_2O_4$ material [288].

Carbon dot-modified TiO_2 NPs and nanotubes produced H_2 at the rate of $75.5 \text{ mmol}\cdot\text{h}^{-1}\text{g}^{-1}$ and $246.1 \text{ mmol}\cdot\text{h}^{-1}\text{g}^{-1}$. One percent Carbon fiber CFs in the CuO /CFs/ TiO_2 composite photocatalyst resulted in a substantially higher photocatalytic HER of $2000 \text{ mmol}\cdot\text{h}^{-1}\text{g}^{-1}$ in 10% ethanol solution under a 300W xenon lamp, more than 45 times than TiO_2 and 2 times more than CuO / TiO_2 . Under visible-light irradiation, a 0.50 wt% CFs/ TiO_2 photocatalyst produced $6.03 \text{ mmol}\cdot\text{h}^{-1}\text{g}^{-1}$ of H_2 compared to $0.71 \text{ mmol}\cdot\text{h}^{-1}\text{g}^{-1}$ for CdS / TiO_2 . Photocatalysts that use CNMs as their support materials have a new lease of life thanks to

single-atom technology [145]. The HER of the N-doped CDs (NCDs)-based photocatalyst (Pt/NCDs/TiO₂) is 175.3 mmol·h⁻¹ cm⁻², which is 17 and 4 times more than neat TiO₂ and NCDs/TiO₂, respectively, for the photocatalyst created by adding a single Pt atom to NCDs and then hybridizing it with TiO₂. The Pt atomic efficiency is maximized, and charge transferability is increased by the interaction of the single Pt atom with N/CDs [289].

Zinc sulfide-carbon dot ZnS/CD nanocomposites display a greater hydrogen evolution rate than the bare ZnS nanospheres, up to 3.2 times higher than that rate. The hydrogen production rate of ZnS nanospheres is 198 mmol·h⁻¹ g⁻¹ and increases in all the ZnS/carbon nanomaterials [15]. A tabularized summary of CQD-based photocatalysts for H₂ production is given in Table 7.

Table 7. H₂ production rate of carbon quantum dot-based composites.

Photocatalyst	Cocatalyst	Sacrificial Agent	Light Source	H ₂ Activity	Reference
CQDs	None	Water	Xenon lamp	423.7 μmol h ⁻¹ g ⁻¹	[87]
CQDs/WO ₃	Pt	Methanol	Xenon lamp	1330 mmol·h ⁻¹ g ⁻¹	[92]
ZnS/CDs	None	Water	Xenon lamp	630.6 mmol·h ⁻¹ g ⁻¹	[15]
CuO/CF/TiO ₂	CuO	Ethanol	Xenon lamp	2000 μmol h ⁻¹ g ⁻¹	[290]
CdS/TiO ₂	None	None	Visible light	0.71 μmol h ⁻¹ g ⁻¹	[291]
C ₆₀ /CdS/TiO ₂	None	None	Visible light	6.03 μmol h ⁻¹ g ⁻¹	[291]
CQDs/-TiO ₂	Pt	Methanol	Xenon lamp	7.42 mmol·h ⁻¹ g ⁻¹	[85]

5. Factors Influencing Properties of Carbon-Based Nanomaterials in Photocatalytic H₂ Evaluation

Understanding the factors and problems that influence the performance of carbon-based photocatalysts for H₂ evaluation reactions is critical. The photocatalyst performance of H₂ production is highly dependent on the dimensions of the carbonaceous materials, the types of defects present, the number of layers, chemical functionalities, the conductivity of the carbon material and the interfacial contact area amid semiconductor and carbon materials. To maximize photocatalytic H₂ generation using carbon materials, reasonable procedures are employed to regulate the carbon materials' structural and property effects.

5.1. Doping

The doping of pristine CNMs with heteroatom can increase their activity as catalysts. By introducing defect sites, heteroatoms can change the physiochemical properties of CNMs and improve active reaction sites [292]. Doping carbon materials with heteroatom also controls their electrical conductivity, electronic structure, and metal or semiconductor-like properties [293]. Doping CNMs with a heteroatom induces a positive or negative charge in the carbon atoms near the dopants, depending on their relative placement and mismatch in electronegativity. That, in turn, causes a shift in the charge distribution in CNMs. Charge variation impacts many physical and chemical properties, including effective surface area, active reaction sites, and electrical conductivity. It can govern charge transfer on the catalytic surface and affect the CNM-based photocatalyst performance [294]. The technology that regulates and detects the atomic level, composition, and catalysis center is still a mystery, despite the progress that has been made in heteroatom doping. Nonmetallic elements are the main focus of the most recent research on heteroatom doping in CNMs for photocatalytic H₂ generation. Heteroatom doping introduces defects and vacancies in nanomaterials. It is challenging to detect the specific heteroatom, vacancies, or defects that contribute to CNM catalysis [118,295]. Using a modified Hummer's process, N-doped graphene quantum dots were fabricated by oxidizing GO in NH₃ at 500 °C. The nitrogen-doped GO material is metal-free photocatalysts and exhibits p- and n-type conductivities, constructing a charge transfer route within the molecule using the Z-scheme. The p-type conductivity produced in oxygen functional groups promotes hydrogen evolution, whereas n-type conductivity promotes oxygen evolution. However, the activity was not relatively as high as that of the composite photocatalyst made of N-doped graphene oxide [119]. A

facile synthesis of phosphorous-doped graphene P/G through the thermal breakdown of H_2PO_4^- at 900 °C under an argon atmosphere for photocatalytic H_2 production is reported [295]. The p-doping led to the transformation of graphene with a zero bandgap into semiconducting graphene, which displayed photocatalytic activity in both the visible and ultraviolet spectra. Triethanolamine as sacrificial agent and Pt as cocatalyst produced $282 \text{ mol h}^{-1} \text{ g}^{-1} \text{ H}_2$ under UV-Vis irradiation.

5.2. Defects

The photocatalytic efficacy of the carbonaceous catalyst can be improved by using defects present on the material surface, particularly the intrinsic defects of the catalyst [296]. Nanomaterials contain defects on multiple scales, including point, line, plane, and volume. In addition, the point defects can be further subdivided according to their location and composition into vacancies, interstitial atoms, and impurities [297]. Realistically, it is not easy to produce defect-free CNMs. The defects in the material can affect the CNMs' electrical and surface properties. The photocatalytic reaction is greatly influenced by the distribution of electron density and charge in CNMs due to defects. The active sites created by these defects can be used as active centers for photocatalytic reactions [298]. It is also possible that the presence of oxygen functionalities and other non-metallic moieties in CNMs lends even more credence to their use for effective H_2 generation [299]. Some advanced CNMs own many intrinsic defects. Defects in graphyne, the new "wonder" material following graphene, alter the efficacy of its photocatalytic hydrogen evolution, although there is not enough study on this. Finding innovative, controllable approaches to address problems caused is more crucial; many incisive and exciting studies have been published; it is still tough to prepare CNMs with different defects under controlled conditions. Controlling defects may make things easier to understand their impact on photocatalytic performance. Most of the reported defective CNMs up to this point were created by annealing or etching [300,301]. Still, it is challenging to discuss the relationship between defects and photocatalytic activity in detail since these techniques cannot precisely control the defects produced.

5.3. Dimensions

The efficacy of a photocatalytic material is highly correlated with the size of the materials. Based on their size, zero-dimensional CNMs have dual photocatalytic and cocatalytic applications. For example, CQDs' photocatalytic properties are typically related with their optical possessions of light absorption and scattering. Decreasing the size of CQDs probably increases charge recombination because e^-/h^+ pairs are created in a compact volume [302,303]. Developing CQD-modified nanocomposite materials will limit control recombination. It is a productive approach to getting over 0D CNMs restriction. Due to their high specific surface area, the 1D CNMs photocatalytic systems have numerous advantages over the 0D CNM system. In 1D CNMs, many active centers are available for photocatalytic reactions because of their exceptional light absorption and scattering efficiency.

Additionally, high-efficiency charge transfer is possible with 1D CNMs, favorably affecting the speed of hydrogen evolution [304,305]. However, the current methods of producing and exploiting 1D material for photocatalytic H_2 production involve essential modifications for practical application. The 2D CNMs possess high photochemical stability, specific surface area, exceptional mechanical and optical properties, and the potential to be used in advanced photocatalytic systems. Improving H_2 generation efficiency and mass transfer performance are the biggest challenges in 2D CNM photocatalysis [9,306]. 2D CNMs possess several advantages over 0D and 1D CNMs in developing and producing efficient photocatalytic H_2 systems. The 2D CNMs can shift the borders of the conduction band and valence bands' borders and efficiently absorb solar radiation, resulting in the recurrent reflection and scattering of photons [245]. The 0D and 1D CNMs only transfer charge one way, whereas 2D CNMs transfer charge in multiple directions, which makes H_2

evolution much more efficient. The photoinduced electron mobility at the photocatalyst surface is affected by the thickness of 2D CNMs, making it an important parameter to evaluate. For 2D photocatalytic systems, this is the fundamental issue.

6. Conclusions

The major challenges of the present day include climate change and the energy crisis. Researchers are looking for energy sources other than fossil fuels, because fossil fuels contribute to the production of greenhouse gases. Hydrogen is a renewable source of energy with widespread potential; however, there are challenges associated with its industrial production and storage. The photocatalytic synthesis of hydrogen from carbon materials is an interesting and potentially useful energy technology. There has been extensive research into the potential of carbon materials, including CNTs, graphene, graphene oxide, graphitic carbon nitride, C₆₀, carbon quantum dots, etc., to outperform semiconductor photocatalysts in H₂ production. Carbon-based nanomaterials require additional reliable and low-cost preparation methods for photocatalytic H₂ evolution. This review explains how carbon-based composite materials improve semiconductor photocatalysts for PWS as catalyst support, an electron acceptor and transference canal booster, cocatalyst, photosensitizer, photocatalyst, and E_g narrowing effect. This review comprehensively explains how carbon-based composite materials function as a photocatalytic semiconductor for hydrogen production, the WS mechanism, and the chemistry of redox reactions. Also, how heteroatom doping, defects, and surface functionalities, etc., can influence the efficiency of carbon photocatalysts for H₂ production. The challenges faced by the PWS process and future prospects are briefly discussed.

Author Contributions: Conceptualization, R.S.; A.I. and M.E.A.Z.; project administration, M.E.A.Z.; supervision and resources, R.S.; data curation and visualization, A.A.; writing—original draft preparation, M.A.R., S.A.A.-H., A.I. and S.A.; writing—review and editing, M.A.R., R.S., A.I., and M.E.A.Z.; funding acquisition, S.A.A.-H., A.I. All authors have read and agreed to the published version of the manuscript.

Funding: The authors extend their appreciation to the Deanship of Scientific Research at Imam Mohammad Ibn Saud Islamic University for funding this work through Research Group No. RG 21-09-77.

Data Availability Statement: Data are available in the manuscript.

Acknowledgments: Authors acknowledge the support and literature facilities provided by the Government College University Faisalabad (GCUF)-Faisalabad and UOL Sargodha Campus-Sargodha-Pakistan.

Conflicts of Interest: The authors declare no conflict of interest.

References

1. Su, T.; Shao, Q.; Qin, Z.; Guo, Z.; Wu, Z. Role of Interfaces in Two-Dimensional Photocatalyst for Water Splitting. *ACS Catal.* **2018**, *8*, 2253–2276. [[CrossRef](#)]
2. Liang, Q.; Li, Z.; Huang, Z.-H.; Kang, F.; Yang, Q.-H. Holey Graphitic Carbon Nitride Nanosheets with Carbon Vacancies for Highly Improved Photocatalytic Hydrogen Production. *Adv. Funct. Mater.* **2015**, *25*, 6885–6892. [[CrossRef](#)]
3. Fang, J.; Fan, H.; Li, M.; Long, C. Nitrogen self-doped graphitic carbon nitride as efficient visible light photocatalyst for hydrogen evolution. *J. Mater. Chem. A* **2015**, *3*, 13819–13826. [[CrossRef](#)]
4. Caspeta, L.; Buijs, N.A.A.; Nielsen, J. The role of biofuels in the future energy supply. *Energy Environ. Sci.* **2013**, *6*, 1077–1082. [[CrossRef](#)]
5. Turhal, S.; Turanbaev, M.; Argun, H. Hydrogen production from melon and watermelon mixture by dark fermentation. *Int. J. Hydrog. Energy* **2019**, *44*, 18811–18817. [[CrossRef](#)]
6. Reddy, C.V.; Reddy, K.R.; Harish, V.V.N.; Shim, J.; Shankar, M.V.; Shetti, N.P.; Aminabhavi, T.M. Metal-organic frameworks (MOFs)-based efficient heterogeneous photocatalysts: Synthesis, properties and its applications in photocatalytic hydrogen generation, CO₂ reduction and photodegradation of organic dyes. *Int. J. Hydrog. Energy* **2020**, *45*, 7656–7679. [[CrossRef](#)]
7. Liao, C.-H.; Huang, C.-W.; Wu, J.C.S. Hydrogen Production from Semiconductor-based Photocatalysis via Water Splitting. *Catalysts* **2012**, *2*, 490–516. [[CrossRef](#)]

8. Daulbayev, C.; Sultanov, F.; Bakbolat, B.; Daulbayev, O. 0D, 1D and 2D nanomaterials for visible photoelectrochemical water splitting. A Review. *Int. J. Hydrog. Energy* **2020**, *45*, 33325–33342. [[CrossRef](#)]
9. Gan, X.; Lei, D.; Wong, K.-Y. Two-dimensional layered nanomaterials for visible-light-driven photocatalytic water splitting. *Mater. Today Energy* **2018**, *10*, 352–367. [[CrossRef](#)]
10. Suryawanshi, A.; Dhanasekaran, P.; Mhamane, D.; Kelkar, S.; Patil, S.; Gupta, N.; Ogale, S. Doubling of photocatalytic H₂ evolution from g-C₃N₄ via its nanocomposite formation with multiwall carbon nanotubes: Electronic and morphological effects. *Int. J. Hydrogen Energy* **2012**, *37*, 9584–9589. [[CrossRef](#)]
11. Tian, J.; Liu, Q.; Asiri, A.M.; Alamry, K.A.; Sun, X. Ultrathin graphitic C₃N₄ nanosheets/graphene composites: Efficient organic electrocatalyst for oxygen evolution reaction. *ChemSusChem* **2014**, *7*, 2125–2130. [[CrossRef](#)] [[PubMed](#)]
12. Pachaiappan, R.; Rajendran, S.; Kumar, P.S.; Vo, D.-V.N.; Hoang, T.K.A.; Cornejo-Ponce, L. Recent advances in carbon nitride-based nanomaterials for hydrogen production and storage. *Int. J. Hydrogen Energy* **2021**, *47*, 37490–37516. [[CrossRef](#)]
13. Reddy, C.V.; Reddy, K.R.; Shetti, N.P.; Shim, J.; Aminabhavi, T.M.; Dionysiou, D.D. Hetero-nanostructured metal oxide-based hybrid photocatalysts for enhanced photoelectrochemical water splitting—A review. *Int. J. Hydrogen Energy* **2020**, *45*, 18331–18347. [[CrossRef](#)]
14. Mishra, A.; Mehta, A.; Basu, S.; Shetti, N.P.; Reddy, K.R.; Aminabhavi, T.M. Graphitic carbon nitride (g-C₃N₄)-based metal-free photocatalysts for water splitting: A review. *Carbon* **2019**, *149*, 693–721. [[CrossRef](#)]
15. Wang, J.; Lim, Y.F.; Wei Ho, G. Carbon-ensemble-manipulated ZnS heterostructures for enhanced photocatalytic H₂ evolution. *Nanoscale* **2014**, *6*, 9673–9680. [[CrossRef](#)]
16. Qazi, U.Y.; Javaid, R.; Zahid, M.; Tahir, N.; Afzal, A.; Lin, X.M. Bimetallic NiCoNiCoO₂ nano-heterostructures embedded on copper foam as a self-supported bifunctional electrode for water oxidation and hydrogen production in alkaline media. *Int. J. Hydrogen Energy* **2021**, *46*, 18936–18948. [[CrossRef](#)]
17. Zhang, Y.; Lighthart, D.A.J.M.; Quek, X.-Y.; Gao, L.; Hensen, E.J.M. Influence of Rh nanoparticle size and composition on the photocatalytic water splitting performance of Rh/graphitic carbon nitride. *Int. J. Hydrogen Energy* **2014**, *39*, 11537–11546. [[CrossRef](#)]
18. Yu, M.; Yuan, X.; Guo, J.; Tang, N.; Ye, S.; Liang, J.; Jiang, L. Selective graphene-like metal-free 2D nanomaterials and their composites for photocatalysis. *Chemosphere* **2021**, *284*, 131254. [[CrossRef](#)]
19. Wang, G.; Chen, T.; Liu, S.; Wang, F.; Li, M.; Xie, M.; Wang, J.; Xiang, Y.; Han, W. Construction of TiO₂-MnO₂ 0D-2D nanostructured heterojunction for enhanced photocatalytic hydrogen production. *Dalton Trans* **2021**, *50*, 8711–8717. [[CrossRef](#)]
20. Wang, S.; Zhao, L.; Bai, L.; Yan, J.; Jiang, Q.; Lian, J. Enhancing Photocatalytic Activity of Disorder-Engineered C/TiO₂ and TiO₂ Nanoparticles. *J. Mater. Chem. A* **2014**, *2*, 7439–7445. [[CrossRef](#)]
21. Li, N.; Ma, Y.; Wang, B.; Huang, Y.; Wu, Y.; Yang, X.; Chen, Y. Synthesis of semiconducting SWNTs by arc discharge and their enhancement of water splitting performance with TiO₂ photocatalyst. *Carbon* **2011**, *49*, 5132–5141. [[CrossRef](#)]
22. Kundu, S.; Bramhaiah, K.; Bhattacharyya, S. Carbon-based nanomaterials: In the quest of alternative metal-free photocatalysts for solar water splitting. *Nanoscale Adv.* **2020**, *2*, 5130–5151. [[CrossRef](#)] [[PubMed](#)]
23. Sudhaik, A.; Raizada, P.; Shandilya, P.; Jeong, D.-Y.; Lim, J.-H.; Singh, P. Review on fabrication of graphitic carbon nitride based efficient nanocomposites for photodegradation of aqueous phase organic pollutants. *J. Ind. Eng. Chem.* **2018**, *67*, 28–51. [[CrossRef](#)]
24. Monga, D.; Basu, S. Enhanced photocatalytic degradation of industrial dye by g-C₃N₄/TiO₂ nanocomposite: Role of shape of TiO₂. *Adv. Powder Technol.* **2019**, *30*, 1089–1098. [[CrossRef](#)]
25. Sharma, R.; Sharma, A.K.; Sharma, V.; Harkin-Jones, E. Synthesis of carbon nanotubes by arc-discharge and chemical vapor deposition method with analysis of its morphology, dispersion and functionalization characteristics. *Cogent Eng.* **2015**, *2*, 1094017. [[CrossRef](#)]
26. Li, Y.-N.; Chen, Z.-Y.; Wang, M.-Q.; Zhang, L.-z.; Bao, S.-J. Interface engineered construction of porous g-C₃N₄/TiO₂ heterostructure for enhanced photocatalysis of organic pollutants. *Appl. Surf. Sci.* **2018**, *440*, 229–236. [[CrossRef](#)]
27. Ghasempour, R.; Narei, H. CNT Basics and Characteristics. In *Carbon Nanotube-Reinforced Polymers*; Elsevier: Amsterdam, The Netherlands, 2018; pp. 1–24.
28. He, Y.; Luo, S.; Hu, X.; Cheng, Y.; Huang, Y.; Chen, S.; Fu, M.; Jia, Y.; Liu, X. NH₂-MIL-125(Ti) encapsulated with in situ-formed carbon nanodots with up-conversion effect for improving photocatalytic NO removal and H₂ evolution. *Chem. Eng. J.* **2021**, *420*, 127643. [[CrossRef](#)]
29. Xiong, S.; Tang, R.; Gong, D.; Deng, Y.; Zheng, J.; Li, L.; Zhou, Z.; Yang, L.; Su, L. Environmentally-friendly carbon nanomaterials for photocatalytic hydrogen production. *Chin. J. Catal.* **2022**, *43*, 1719–1748. [[CrossRef](#)]
30. Porto, L.S.; Silva, D.N.; de Oliveira, A.E.F.; Pereira, A.C.; Borges, K.B. Carbon nanomaterials: Synthesis and applications to development of electrochemical sensors in determination of drugs and compounds of clinical interest. *Rev. Anal. Chem.* **2020**, *3*. [[CrossRef](#)]
31. Azizi-Lalabadi, M.; Hashemi, H.; Feng, J.; Jafari, S.M. Carbon nanomaterials against pathogens; the anti-microbial activity of carbon nanotubes, graphene/graphene oxide, fullerenes, and their nanocomposites. *Adv. Colloid Interface Sci.* **2020**, *284*, 102250. [[CrossRef](#)]
32. Fujishima, A.; Honda, K. Electrochemical photolysis of water at a semiconductor electrode. *Nature* **1972**, *238*, 37–38. [[CrossRef](#)] [[PubMed](#)]
33. Bard, A.J. Photoelectrochemistry and heterogeneous photo-catalysis at semiconductors. *J. Photochem.* **1979**, *10*, 59–75. [[CrossRef](#)]

34. Li, R.; Li, C. Photocatalytic Water Splitting on Semiconductor-Based Photocatalysts. *Adv. Catal.* **2017**, *60*, 1–57.
35. Patel, S.B.; Tripathi, A.; Vyas, A.P. Recent development in the structural modification of graphitic carbon nitride for sustainable photocatalysis: Advances, challenges and opportunities. *Environ. Nanotechnol. Monit. Manag.* **2021**, *16*, 100589. [[CrossRef](#)]
36. Kong, D.; Zheng, Y.; Kobielski, M.; Wang, Y.; Bai, Z.; Macyk, W.; Wang, X.; Tang, J. Recent advances in visible light-driven water oxidation and reduction in suspension systems. *Mater. Today* **2018**, *21*, 897–924. [[CrossRef](#)]
37. Li, X.; Yu, J.; Low, J.; Fang, Y.; Xiao, J.; Chen, X. Engineering heterogeneous semiconductors for solar water splitting. *J. Mater. Chem. A* **2015**, *3*, 2485–2534. [[CrossRef](#)]
38. Tong, H.; Ouyang, S.; Bi, Y.; Umezawa, N.; Oshikiri, M.; Ye, J. Nano-photocatalytic materials: Possibilities and challenges. *Adv. Mater.* **2012**, *24*, 229–251. [[CrossRef](#)]
39. Moniz, S.J.A.; Shevlin, S.A.; Martin, D.J.; Guo, Z.-X.; Tang, J. Visible-light driven heterojunction photocatalysts for water splitting—A critical review. *Energy Environ. Sci.* **2015**, *8*, 731–759. [[CrossRef](#)]
40. Xie, G.; Zhang, K.; Guo, B.; Liu, Q.; Fang, L.; Gong, J.R. Graphene-based materials for hydrogen generation from light-driven water splitting. *Adv. Mater.* **2013**, *25*, 3820–3839. [[CrossRef](#)]
41. Hisatomi, T.; Kubota, J.; Domen, K. Recent advances in semiconductors for photocatalytic and photoelectrochemical water splitting. *Chem. Soc. Rev.* **2014**, *43*, 7520–7535. [[CrossRef](#)]
42. Mishra, A.; Basu, S.; Shetti, N.P.; Reddy, K.R.; Aminabhavi, T.M. Photocatalysis of Graphene and Carbon Nitride-Based Functional Carbon Quantum Dots. In *Nanoscale Materials in Water Purification*; Elsevier: Amsterdam, The Netherlands, 2019; pp. 759–781.
43. Tachibana, Y.; Vayssieres, L.; Durrant, J.R. Artificial photosynthesis for solar water splitting. *Nat. Photonics* **2012**, *6*, 511–518. [[CrossRef](#)]
44. Maeda, K. Photocatalytic water splitting using semiconductor particles: History and recent developments. *J. Photochem. Photobiol. C Photochem. Rev.* **2011**, *12*, 237–268. [[CrossRef](#)]
45. Meng, A.; Zhang, L.; Cheng, B.; Yu, J. Dual Cocatalysts in TiO₂ Photocatalysis. *Adv. Mater.* **2019**, *31*, e1807660. [[CrossRef](#)] [[PubMed](#)]
46. Linsebigler, A.L.; Lu, G.; Yates, J.J.T. Photocatalysis on TiO_n Surfaces: Principles, Mechanisms, and Selected Results. *Chem. Rev.* **1995**, *95*, 735–758. [[CrossRef](#)]
47. Chen, X.; Mao, S.S. Titanium Dioxide Nanomaterials: Synthesis, Properties, Modifications, and Applications. *Chem. Rev.* **2007**, *107*, 2891–2959. [[CrossRef](#)]
48. Chen, X.; Shen, S.; Guo, L.; Mao, S.S. Semiconductor-based Photocatalytic Hydrogen Generation. *Chem. Rev.* **2010**, *110*, 6503–6570. [[CrossRef](#)] [[PubMed](#)]
49. Xiao, N.; Li, S.; Li, X.; Ge, L.; Gao, Y.; Li, N. The roles and mechanism of cocatalysts in photocatalytic water splitting to produce hydrogen. *Chin. J. Catal.* **2020**, *41*, 642–671. [[CrossRef](#)]
50. Xiang, Q.; Cheng, B.; Yu, J. Graphene-Based Photocatalysts for Solar-Fuel Generation. *Angew. Chem. Int. Ed. Engl.* **2015**, *54*, 11350–11366. [[CrossRef](#)]
51. Wu, Q.; Zhu, M.; Cao, J.; Wang, X.; Liu, Y.; Xiang, C.; Shao, M.; Tian, H.; Kang, Z. Metal-Free Catalyst with Large Carbon Defects for Efficient Direct Overall Water Splitting in Air at Room Pressure. *ACS Appl. Mater. Interfaces* **2020**, *12*, 30280–30288. [[CrossRef](#)]
52. Lin, Q.; Zhang, J.; Lv, W.; Ma, J.; He, Y.; Kang, F.; Yang, Q.H. A Functionalized Carbon Surface for High-Performance Sodium-Ion Storage. *Small* **2020**, *16*, e1902603. [[CrossRef](#)]
53. Wen, J.; Xie, J.; Yang, Z.; Shen, R.; Li, H.; Luo, X.; Chen, X.; Li, X. Fabricating the Robust g-C₃N₄ Nanosheets/Carbons/NiS Multiple Heterojunctions for Enhanced Photocatalytic H₂ Generation: An Insight into the Trifunctional Roles of Nanocarbons. *ACS Sustain. Chem. Eng.* **2017**, *5*, 2224–2236. [[CrossRef](#)]
54. Chai, B.; Peng, T.; Zhang, X.; Mao, J.; Li, K.; Zhang, X. Synthesis of C₆₀-decorated SWCNTs (C₆₀-d-CNTs) and its TiO₂-based nanocomposite with enhanced photocatalytic activity for hydrogen production. *Dalton Trans.* **2013**, *42*, 3402–3409. [[CrossRef](#)] [[PubMed](#)]
55. Zhu, T.; Wu, H.B.; Wang, Y.; Xu, R.; Lou, X.W.D. Formation of 1D Hierarchical Structures Composed of Ni₃S₂ Nanosheets on CNTs Backbone for Supercapacitors and Photocatalytic H₂ Production. *Adv. Energy Mater.* **2012**, *2*, 1497–1502. [[CrossRef](#)]
56. Huo, J.; Zeng, H. A novel triphenylamine functionalized bithiazole–metal complex with C₆₀ for photocatalytic hydrogen production under visible light irradiation. *J. Mater. Chem. A* **2015**, *3*, 6258–6264. [[CrossRef](#)]
57. Shi, W.; Guo, F.; Li, M.; Shi, Y.; Wu, M.; Tang, Y. Enhanced visible-light-driven photocatalytic H₂ evolution on the novel nitrogen-doped carbon dots/CuBi₂O₄ microrods composite. *J. Alloys Compd.* **2019**, *775*, 511–517. [[CrossRef](#)]
58. Hareesh, K.; Dhole, S.D.; Phase, D.M.; Williams, J.F. One-step bacterial assisted synthesis of CdS/rGO nanocomposite as Hydrogen production catalyst. *Mater. Res. Bull.* **2019**, *110*, 82–89. [[CrossRef](#)]
59. Dan, M.; Xiang, J.; Wu, F.; Yu, S.; Cai, Q.; Ye, L.; Ye, Y.; Zhou, Y. Rich active-edge-site MoS₂ anchored on reduction sites in metal sulfide heterostructure: Toward robust visible light photocatalytic hydrogen sulphide splitting. *Appl. Catal. B Environ.* **2019**, *256*, 117870. [[CrossRef](#)]
60. Deng, D.; Novoselov, K.S.; Fu, Q.; Zheng, N.; Tian, Z.; Bao, X. Catalysis with two-dimensional materials and their heterostructures. *Nat. Nanotechnol.* **2016**, *11*, 218–230. [[CrossRef](#)]
61. Hamza, M.A.; El-Shazly, A.N.; Tolba, S.A.; Allam, N.K. Novel Bi-based photocatalysts with unprecedented visible light-driven hydrogen production rate: Experimental and DFT insights. *Chem. Eng. J.* **2020**, *384*, 123351. [[CrossRef](#)]

62. Chen, P.; Wang, L.; Wang, P.; Kostka, A.; Wark, M.; Muhler, M.; Beranek, R. CNT-TiO₂- δ Composites for Improved Co-Catalyst Dispersion and Stabilized Photocatalytic Hydrogen Production. *Catalysts* **2015**, *5*, 270–285. [[CrossRef](#)]
63. MamathaKumari, M.; Kumar, D.P.; Haridoss, P.; DurgaKumari, V.; Shankar, M. Nanohybrid of titania/carbon nanotubes-nanohorns: A promising photocatalyst for enhanced hydrogen production under solar irradiation. *Int. J. Hydrog. Energy* **2015**, *40*, 1665–1674. [[CrossRef](#)]
64. Wang, L.; Yao, Z.; Jia, F.; Chen, B.; Jiang, Z. A facile synthesis of Zn_xCd_{1-x}S/CNTs nanocomposite photocatalyst for H₂ production. *Dalton Trans.* **2013**, *42*, 9976–9981. [[CrossRef](#)] [[PubMed](#)]
65. Kim, Y.K.; Kim, M.; Hwang, S.-H.; Lim, S.K.; Park, H.; Kim, S. CdS-loaded flexible carbon nanofiber mats as a platform for solar hydrogen production. *Int. J. Hydrogen Energy* **2015**, *40*, 136–145. [[CrossRef](#)]
66. Kim, M.; Razzaq, A.; Kim, Y.K.; Kim, S.; In, S.-I. Synthesis and characterization of platinum modified TiO₂-embedded carbon nanofibers for solar hydrogen generation. *RSC Adv.* **2014**, *4*, 51286–51293. [[CrossRef](#)]
67. Wang, J.; Huang, H.; Xu, Z.; Kou, J.; Lu, C. The potential of carbon-based materials for photocatalytic application. *Curr. Org. Chem.* **2014**, *18*, 1346–1364. [[CrossRef](#)]
68. Julkapli, N.M.; Bagheri, S. Graphene supported heterogeneous catalysts: An overview. *Int. J. Hydrogen Energy* **2015**, *40*, 948–979. [[CrossRef](#)]
69. Li, Y.; Wang, H.; Peng, S. Tunable photodeposition of MoS₂ onto a composite of reduced graphene oxide and CdS for synergic photocatalytic hydrogen generation. *J. Phys. Chem. C* **2014**, *118*, 19842–19848. [[CrossRef](#)]
70. Li, Q.; Guo, B.; Yu, J.; Ran, J.; Zhang, B.; Yan, H.; Gong, J.R. Highly efficient visible-light-driven photocatalytic hydrogen production of CdS-cluster-decorated graphene nanosheets. *J. Am. Chem. Soc.* **2011**, *133*, 10878–10884. [[CrossRef](#)]
71. Shen, S.; Ma, A.; Tang, Z.; Han, Z.; Wang, M.; Wang, Z.; Zhi, L.; Yang, J. Facile synthesis of Zn_{0.5}Cd_{0.5}S ultrathin nanorods on reduced graphene oxide for enhanced photocatalytic hydrogen evolution under visible light. *ChemCatChem* **2015**, *7*, 609–615. [[CrossRef](#)]
72. Yang, J.; Wang, D.; Han, H.; Li, C. Roles of cocatalysts in photocatalysis and photoelectrocatalysis. *Acc. Chem. Res.* **2013**, *46*, 1900–1909. [[CrossRef](#)]
73. Ran, J.; Zhang, J.; Yu, J.; Jaroniec, M.; Qiao, S.Z. Earth-abundant cocatalysts for semiconductor-based photocatalytic water splitting. *Chem. Soc. Rev.* **2014**, *43*, 7787–7812. [[CrossRef](#)]
74. Khan, G.; Choi, S.K.; Kim, S.; Lim, S.K.; Jang, J.S.; Park, H. Carbon nanotubes as an auxiliary catalyst in heterojunction photocatalysis for solar hydrogen. *Appl. Catal. B Environ.* **2013**, *142*, 647–653. [[CrossRef](#)]
75. Wen, J.; Li, X.; Li, H.; Ma, S.; He, K.; Xu, Y.; Fang, Y.; Liu, W.; Gao, Q. Enhanced visible-light H₂ evolution of g-C₃N₄ photocatalysts via the synergetic effect of amorphous NiS and cheap metal-free carbon black nanoparticles as co-catalysts. *Appl. Surf. Sci.* **2015**, *358*, 204–212. [[CrossRef](#)]
76. Gan, Z.; Wu, X.; Meng, M.; Zhu, X.; Yang, L.; Chu, P.K. Photothermal contribution to enhanced photocatalytic performance of graphene-based nanocomposites. *ACS Nano* **2014**, *8*, 9304–9310. [[CrossRef](#)]
77. Sun, S.; Wang, W.; Jiang, D.; Zhang, L.; Zhou, J. Infrared light induced photoelectrocatalytic application via graphene oxide coated thermoelectric device. *Appl. Catal. B Environ.* **2014**, *158*, 136–139. [[CrossRef](#)]
78. Xiang, Q.; Yu, J.; Jaroniec, M. Synergetic effect of MoS₂ and graphene as cocatalysts for enhanced photocatalytic H₂ production activity of TiO₂ nanoparticles. *J. Am. Chem. Soc.* **2012**, *134*, 6575–6578. [[CrossRef](#)]
79. Yu, J.; Yang, B.; Cheng, B. Noble-metal-free carbon nanotube-Cd_{0.1}Zn_{0.9}S composites for high visible-light photocatalytic H₂-production performance. *Nanoscale* **2012**, *4*, 2670–2677. [[CrossRef](#)]
80. Wang, P.; Dimitrijevic, N.M.; Chang, A.Y.; Schaller, R.D.; Liu, Y.; Rajh, T.; Rozhkova, E.A. Photoinduced electron transfer pathways in hydrogen-evolving reduced graphene oxide-boosted hybrid nano-bio catalyst. *ACS Nano* **2014**, *8*, 7995–8002. [[CrossRef](#)]
81. Xie, S.; Su, H.; Wei, W.; Li, M.; Tong, Y.; Mao, Z. Remarkable photoelectrochemical performance of carbon dots sensitized TiO₂ under visible light irradiation. *J. Mater. Chem. A* **2014**, *2*, 16365–16368. [[CrossRef](#)]
82. Zhang, X.; Huang, H.; Liu, J.; Liu, Y.; Kang, Z. Carbon quantum dots serving as spectral converters through broadband upconversion of near-infrared photons for photoelectrochemical hydrogen generation. *J. Mater. Chem. A* **2013**, *1*, 11529–11533. [[CrossRef](#)]
83. Wang, F.; Zheng, M.; Zhu, C.; Zhang, B.; Chen, W.; Ma, L.; Shen, W. Visible light photocatalytic H₂-production activity of wide band gap ZnS nanoparticles based on the photosensitization of graphene. *Nanotechnology* **2015**, *26*, 345402. [[CrossRef](#)] [[PubMed](#)]
84. Martindale, B.C.; Hutton, G.A.; Caputo, C.A.; Reisner, E. Solar hydrogen production using carbon quantum dots and a molecular nickel catalyst. *J. Am. Chem. Soc.* **2015**, *137*, 6018–6025. [[CrossRef](#)] [[PubMed](#)]
85. Tian, J.; Leng, Y.; Zhao, Z.; Xia, Y.; Sang, Y.; Hao, P.; Zhan, J.; Li, M.; Liu, H. Carbon quantum dots/hydrogenated TiO₂ nanobelt heterostructures and their broad spectrum photocatalytic properties under UV, visible, and near-infrared irradiation. *Nano Energy* **2015**, *11*, 419–427. [[CrossRef](#)]
86. Dai, K.; Peng, T.; Ke, D.; Wei, B. Photocatalytic hydrogen generation using a nanocomposite of multi-walled carbon nanotubes and TiO₂ nanoparticles under visible light irradiation. *Nanotechnology* **2009**, *20*, 125603. [[CrossRef](#)]
87. Yang, P.; Zhao, J.; Wang, J.; Cui, H.; Li, L.; Zhu, Z. Pure carbon nanodots for excellent photocatalytic hydrogen generation. *RSC Adv.* **2015**, *5*, 21332–21335. [[CrossRef](#)]
88. Yeh, T.F.; Syu, J.M.; Cheng, C.; Chang, T.H.; Teng, H. Graphite oxide as a photocatalyst for hydrogen production from water. *Adv. Funct. Mater.* **2010**, *20*, 2255–2262. [[CrossRef](#)]

89. Xu, L.; Huang, W.-Q.; Wang, L.-L.; Tian, Z.-A.; Hu, W.; Ma, Y.; Wang, X.; Pan, A.; Huang, G.-F. Insights into enhanced visible-light photocatalytic hydrogen evolution of g-C₃N₄ and highly reduced graphene oxide composite: The role of oxygen. *Chem. Mater.* **2015**, *27*, 1612–1621. [[CrossRef](#)]
90. Meng, F.; Li, J.; Cushing, S.K.; Zhi, M.; Wu, N. Solar hydrogen generation by nanoscale p–n junction of p-type molybdenum disulfide/n-type nitrogen-doped reduced graphene oxide. *J. Am. Chem. Soc.* **2013**, *135*, 10286–10289. [[CrossRef](#)]
91. Jiang, X.; Nisar, J.; Pathak, B.; Zhao, J.; Ahuja, R. Graphene oxide as a chemically tunable 2-D material for visible-light photocatalyst applications. *J. Catal.* **2013**, *299*, 204–209. [[CrossRef](#)]
92. Yang, P.; Zhao, J.; Wang, J.; Cao, B.; Li, L.; Zhu, Z. Construction of Z-scheme carbon nanodots/WO₃ with highly enhanced photocatalytic hydrogen production. *J. Mater. Chem. A* **2015**, *3*, 8256–8259. [[CrossRef](#)]
93. Yang, P.; Zhao, J.; Wang, J.; Cao, B.; Li, L.; Zhu, Z. Light-induced synthesis of photoluminescent carbon nanoparticles for Fe³⁺ sensing and photocatalytic hydrogen evolution. *J. Mater. Chem. A* **2015**, *3*, 136–138. [[CrossRef](#)]
94. Yuan, Y.; Gong, X.; Wang, H. The synergistic mechanism of graphene and MoS₂ for hydrogen generation: Insights from density functional theory. *Phys. Chem. Chem. Phys.* **2015**, *17*, 11375–11381. [[CrossRef](#)] [[PubMed](#)]
95. Shaban, Y.A.; Khan, S.U. Visible light active carbon modified n-TiO₂ for efficient hydrogen production by photoelectrochemical splitting of water. *Int. J. Hydrogen Energy* **2008**, *33*, 1118–1126. [[CrossRef](#)]
96. Ye, A.; Fan, W.; Zhang, Q.; Deng, W.; Wang, Y. CdS-graphene and CdS-CNT nanocomposites as visible-light photocatalysts for hydrogen evolution and organic dye degradation. *Catal. Sci. Technol.* **2012**, *2*, 969–978. [[CrossRef](#)]
97. Sun, Z.; Guo, J.; Zhu, S.; Ma, J.; Liao, Y.; Zhang, D. High photocatalytic performance by engineering Bi₂WO₆ nanoneedles onto graphene sheets. *RSC Adv.* **2014**, *4*, 27963–27970. [[CrossRef](#)]
98. Sun, Z.; Guo, J.; Zhu, S.; Mao, L.; Ma, J.; Zhang, D. A high-performance Bi₂WO₆–graphene photocatalyst for visible light-induced H₂ and O₂ generation. *Nanoscale* **2014**, *6*, 2186–2193. [[CrossRef](#)]
99. Geim, A.K.; Novoselov, K.S. The rise of graphene. In *Nanoscience and Technology: A Collection of Reviews from Nature Journals*; World Scientific: Toh Tuck, Singapore, 2010; pp. 11–19.
100. Ferrari, A.C.; Basko, D.M. Raman spectroscopy as a versatile tool for studying the properties of graphene. *Nat. Nanotechnol.* **2013**, *8*, 235–246. [[CrossRef](#)]
101. Tayel, A.; Ramadan, A.; El Seoud, O. Titanium Dioxide/Graphene and Titanium Dioxide/Graphene Oxide Nanocomposites: Synthesis, Characterization and Photocatalytic Applications for Water Decontamination. *Catalysts* **2018**, *8*, 491. [[CrossRef](#)]
102. Zhu, Y.; Murali, S.; Cai, W.; Li, X.; Suk, J.W.; Potts, J.R.; Ruoff, R.S. Graphene and graphene oxide: Synthesis, properties, and applications. *Adv. Mater.* **2010**, *22*, 3906–3924. [[CrossRef](#)]
103. Ji, X.; Xu, Y.; Zhang, W.; Cui, L.; Liu, J. Review of functionalization, structure and properties of graphene/polymer composite fibers. *Compos. Part A Appl. Sci. Manuf.* **2016**, *87*, 29–45. [[CrossRef](#)]
104. Lavin-Lopez, M.; Valverde, J.; Cuevas, M.; Garrido, A.; Sanchez-Silva, L.; Martinez, P.; Romero-Izquierdo, A. Synthesis and characterization of graphene: Influence of synthesis variables. *Phys. Chem. Chem. Phys.* **2014**, *16*, 2962–2970. [[CrossRef](#)] [[PubMed](#)]
105. Papageorgiou, D.G.; Kinloch, I.A.; Young, R.J. Mechanical properties of graphene and graphene-based nanocomposites. *Prog. Mater. Sci.* **2017**, *90*, 75–127. [[CrossRef](#)]
106. Chen, D.; Feng, H.; Li, J. Graphene oxide: Preparation, functionalization, and electrochemical applications. *Chem. Rev.* **2012**, *112*, 6027–6053. [[CrossRef](#)] [[PubMed](#)]
107. Varghese, J. CuS–ZnS decorated graphene nanocomposites: Synthesis and photocatalytic properties. *J. Phys. Chem. Solids* **2021**, *156*, 109911. [[CrossRef](#)]
108. Diaz-Angulo, J.; Porras, J.; Mueses, M.; Torres-Palma, R.; Hernandez-Ramirez, A.; Machuca-Martinez, F. Coupling of heterogeneous photocatalysis and photosensitized oxidation for diclofenac degradation: Role of the oxidant species. *J. Photochem. Photobiol. A Chem.* **2019**, *383*, 112015. [[CrossRef](#)]
109. Son, S.; Lee, J.M.; Kim, S.-J.; Kim, H.; Jin, X.; Wang, K.K.; Kim, M.; Hwang, J.W.; Choi, W.; Kim, Y.-R. Understanding the relative efficacies and versatile roles of 2D conductive nanosheets in hybrid-type photocatalyst. *Appl. Catal. B Environ.* **2019**, *257*, 117875. [[CrossRef](#)]
110. Dong, C.; Li, X.; Jin, P.; Zhao, W.; Chu, J.; Qi, J. Intersubunit electron transfer (IET) in quantum dots/graphene complex: What features does IET endow the complex with? *J. Phys. Chem. C* **2012**, *116*, 15833–15838. [[CrossRef](#)]
111. Dreyer, D.; Park, S.; Bielawski, C. RS Ruoff The chemistry of graphene oxide *Chem. Soc. Rev.* **2010**, *39*, 228–240. [[CrossRef](#)]
112. Malato, S.; Fernández-Ibáñez, P.; Maldonado, M.I.; Blanco, J.; Gernjak, W. Decontamination and disinfection of water by solar photocatalysis: Recent overview and trends. *Catal. Today* **2009**, *147*, 1–59. [[CrossRef](#)]
113. Zhang, H.; Lv, X.; Li, Y.; Wang, Y.; Li, J. P25-graphene composite as a high performance photocatalyst. *ACS Nano* **2010**, *4*, 380–386. [[CrossRef](#)]
114. Zhang, X.-Y.; Li, H.-P.; Cui, X.-L.; Lin, Y. Graphene/TiO₂ nanocomposites: Synthesis, characterization and application in hydrogen evolution from water photocatalytic splitting. *J. Mater. Chem.* **2010**, *20*, 2801–2806. [[CrossRef](#)]
115. Xu, H.; Ma, L.; Jin, Z. Nitrogen-doped graphene: Synthesis, characterizations and energy applications. *J. Energy Chem.* **2018**, *27*, 146–160. [[CrossRef](#)]
116. Shao, Y.; Zhang, S.; Engelhard, M.H.; Li, G.; Shao, G.; Wang, Y.; Liu, J.; Aksay, I.A.; Lin, Y. Nitrogen-doped graphene and its electrochemical applications. *J. Mater. Chem.* **2010**, *20*, 7491–7496. [[CrossRef](#)]

117. Jin, Z.; Yao, J.; Kittrell, C.; Tour, J.M. Large-scale growth and characterizations of nitrogen-doped monolayer graphene sheets. *Acc Nano* **2011**, *5*, 4112–4117. [[CrossRef](#)] [[PubMed](#)]
118. Lavorato, C.; Primo, A.; Molinari, R.; Garcia, H. N-Doped Graphene Derived from Biomass as a Visible-Light Photocatalyst for Hydrogen Generation from Water/Methanol Mixtures. *Chem. A Eur. J.* **2014**, *20*, 187–194. [[CrossRef](#)]
119. Yeh, T.F.; Teng, C.Y.; Chen, S.J.; Teng, H. Nitrogen-doped graphene oxide quantum dots as photocatalysts for overall water-splitting under visible light illumination. *Adv. Mater.* **2014**, *26*, 3297–3303. [[CrossRef](#)]
120. Zhang, D.; Hu, B.; Guan, D.; Luo, Z. Essential roles of defects in pure graphene/Cu₂O photocatalyst. *Catal. Commun.* **2016**, *76*, 7–12. [[CrossRef](#)]
121. Mateo, D.; Esteve-Adell, I.; Albero, J.; Primo, A.; Garcia, H. Oriented 2.0. 0 Cu₂O nanoplatelets supported on few-layers graphene as efficient visible light photocatalyst for overall water splitting. *Appl. Catal. B Environ.* **2017**, *201*, 582–590. [[CrossRef](#)]
122. Akhavan, O.; Ghaderi, E. Photocatalytic reduction of graphene oxide nanosheets on TiO₂ thin film for photoinactivation of bacteria in solar light irradiation. *J. Phys. Chem. C* **2009**, *113*, 20214–20220. [[CrossRef](#)]
123. Dong, C.; Xing, M.; Lei, J.; Zhang, J. TiO₂/carbon composite nanomaterials for photocatalysis. In *Current Developments in Photocatalysis and Photocatalytic Materials*; Elsevier: Amsterdam, Netherlands, 2020; pp. 303–321.
124. Rivero, M.J.; Iglesias, O.; Ribao, P.; Ortiz, I. Kinetic performance of TiO₂/Pt/reduced graphene oxide composites in the photocatalytic hydrogen production. *Int. J. Hydrogen Energy* **2019**, *44*, 101–109. [[CrossRef](#)]
125. Matsumura, M.; Furukawa, S.; Saho, Y.; Tsubomura, H. Cadmium sulfide photocatalyzed hydrogen production from aqueous solutions of sulfite: Effect of crystal structure and preparation method of the catalyst. *J. Phys. Chem.* **1985**, *89*, 1327–1329. [[CrossRef](#)]
126. Reber, J.F.; Rusek, M. Photochemical hydrogen production with platinized suspensions of cadmium sulfide and cadmium zinc sulfide modified by silver sulfide. *J. Phys. Chem.* **1986**, *90*, 824–834. [[CrossRef](#)]
127. Jha, R.; Dulikravich, G.S.; Chakraborti, N.; Fan, M.; Schwartz, J.; Koch, C.C.; Colaco, M.J.; Poloni, C.; Egorov, I.N. Algorithms for design optimization of chemistry of hard magnetic alloys using experimental data. *J. Alloys Compd.* **2016**, *682*, 454–467. [[CrossRef](#)]
128. Lv, Y.; Yao, W.; Zong, R.; Zhu, Y. Fabrication of wide-range-visible photocatalyst Bi₂WO_{6-x} nanoplates via surface oxygen vacancies. *Sci. Rep.* **2016**, *6*, 19347. [[CrossRef](#)]
129. Das, M.; Datta, J.; Jana, R.; Sil, S.; Halder, S.; Ray, P.P. Synthesis of rGO-Zn_{0.8}Cd_{0.2}S via in situ reduction of GO for the realization of a Schottky diode with low barrier height and highly enhanced photoresponsivity. *New J. Chem.* **2017**, *41*, 5476–5486. [[CrossRef](#)]
130. Zhang, J.; Qi, L.; Ran, J.; Yu, J.; Qiao, S.Z. Ternary NiS/Zn_xCd_{1-x}S/reduced graphene oxide nanocomposites for enhanced solar photocatalytic H₂-production activity. *Adv. Energy Mater.* **2014**, *4*, 1301925. [[CrossRef](#)]
131. Lin, R.; Shen, L.; Ren, Z.; Wu, W.; Tan, Y.; Fu, H.; Zhang, J.; Wu, L. Enhanced photocatalytic hydrogen production activity via dual modification of MOF and reduced graphene oxide on CdS. *Chem. Commun.* **2014**, *50*, 8533–8535. [[CrossRef](#)]
132. Govindan, K.; Suresh, A.; Sakthivel, T.; Murugesan, K.; Mohan, R.; Gunasekaran, V.; Jang, A. Effect of peroxomonosulfate, peroxodisulfate and hydrogen peroxide on graphene oxide photocatalytic performances in methyl orange dye degradation. *Chemosphere* **2019**, *237*, 124479. [[CrossRef](#)]
133. Xia, Y.; Cheng, B.; Fan, J.; Yu, J.; Liu, G. Unraveling Photoexcited Charge Transfer Pathway and Process of CdS/Graphene Nanoribbon Composites toward Visible-Light Photocatalytic Hydrogen Evolution. *Small* **2019**, *15*, 1902459. [[CrossRef](#)]
134. Iijima, S. Helical microtubules of graphitic carbon. *Nature* **1991**, *354*, 56–58. [[CrossRef](#)]
135. Zeng, Q.; Li, Z.; Zhou, Y. Synthesis and Application of Carbon Nanotubes. *J. Nat. Gas Chem.* **2006**, *15*, 235–246. [[CrossRef](#)]
136. Gupta, N.; Gupta, S.M.; Sharma, S.K. Carbon nanotubes: Synthesis, properties and engineering applications. *Carbon Lett.* **2019**, *29*, 419–447. [[CrossRef](#)]
137. Li, Y.; Wang, Z.; Zhao, H.; Yang, M. Composite of TiO₂ nanoparticles and carbon nanotubes loaded on poly(methyl methacrylate) nanofibers: Preparation and photocatalytic performance. *Synth. Met.* **2020**, *269*, 116529. [[CrossRef](#)]
138. Kingston, C.; Zepp, R.; Andrady, A.; Boverhof, D.; Fehir, R.; Hawkins, D.; Roberts, J.; Sayre, P.; Shelton, B.; Sultan, Y.; et al. Release characteristics of selected carbon nanotube polymer composites. *Carbon* **2014**, *68*, 33–57. [[CrossRef](#)]
139. Lehman, J.H.; Terrones, M.; Mansfield, E.; Hurst, K.E.; Meunier, V. Evaluating the characteristics of multiwall carbon nanotubes. *Carbon* **2011**, *49*, 2581–2602. [[CrossRef](#)]
140. Cao, J.; Zhou, J.; Zhang, Y.; Liu, X. A clean and facile synthesis strategy of MoS₂ nanosheets grown on multi-wall CNTs for enhanced hydrogen evolution reaction performance. *Sci. Rep.* **2017**, *7*, 1–8. [[CrossRef](#)]
141. Ma, L.; Dong, X.; Chen, M.; Zhu, L.; Wang, C.; Yang, F.; Dong, Y. Fabrication and water treatment application of carbon nanotubes (CNTs)-based composite membranes: A review. *Membranes* **2017**, *7*, 16. [[CrossRef](#)]
142. Hanaei, H.; Assadi, M.K.; Saidur, R. Highly efficient antireflective and self-cleaning coatings that incorporate carbon nanotubes (CNTs) into solar cells: A review. *Renew. Sustain. Energy Rev.* **2016**, *59*, 620–635. [[CrossRef](#)]
143. Basheer, B.V.; George, J.J.; Siengchin, S.; Parameswaranpillai, J. Polymer grafted carbon nanotubes—Synthesis, properties, and applications: A review. *Nano-Struct. Nano-Objects* **2020**, *22*, 100429. [[CrossRef](#)]
144. Rahmandoust, M.; Ayatollahi, M.R. Carbon nanotubes. In *Characterization of Carbon Nanotube Based Composites under Consideration of Defects*; Springer: Berlin/Heidelberg, Germany, 2016; pp. 5–63.
145. Khare, R.; Bose, S. Carbon Nanotube Based Composites—A Review. *J. Miner. Mater. Charact. Eng.* **2005**, *4*, 31. [[CrossRef](#)]
146. Kim, H.T.; Pathak, V.B.; Pae, K.H.; Lifschitz, A.; Sylla, F.; Shin, J.H.; Hojbota, C.; Lee, S.K.; Sung, J.H.; Lee, H.W.; et al. Stable multi-GeV electron accelerator driven by waveform-controlled PW laser pulses. *Sci. Rep.* **2017**, *7*, 10203. [[CrossRef](#)] [[PubMed](#)]

147. Kharissova, O.V.; Kharisov, B.I. Variations of interlayer spacing in carbon nanotubes. *RSC Adv.* **2014**, *4*, 30807–30815. [[CrossRef](#)]
148. Maniecki, T.; Shtyka, O.; Mierczynski, P.; Ciesielski, R.; Czyilkowska, A.; Leyko, J.; Mitukiewicz, G.; Dubkov, S.; Gromov, D. Carbon Nanotubes: Properties, Synthesis, and Application. *Fibre Chem.* **2019**, *50*, 297–300. [[CrossRef](#)]
149. Mierczynski, P.; Vasilev, K.; Mierczynska, A.; Maniukiewicz, W.; Szyrkowska, M.I.; Maniecki, T.P. Bimetallic Au–Cu, Au–Ni catalysts supported on MWCNTs for oxy-steam reforming of methanol. *Appl. Catal. B Environ.* **2016**, *185*, 281–294. [[CrossRef](#)]
150. Mierczynski, P.; Mierczynska, A.; Maniukiewicz, W.; Maniecki, T.; Vasilev, K. MWCNTs as a catalyst in oxy-steam reforming of methanol. *RSC Adv.* **2016**, *6*, 81408–81413. [[CrossRef](#)]
151. Chernyak, S.; Suslova, E.; Ivanov, A.; Egorov, A.; Maslakov, K.; Savilov, S.; Lunin, V. Co catalysts supported on oxidized CNTs: Evolution of structure during preparation, reduction and catalytic test in Fischer-Tropsch synthesis. *Appl. Catal. A Gen.* **2016**, *523*, 221–229. [[CrossRef](#)]
152. Frank, B.; Zhang, J.; Blume, R.; Schlogl, R.; Su, D.S. Heteroatoms increase the selectivity in oxidative dehydrogenation reactions on nanocarbons. *Angew. Chem. Int. Ed. Engl.* **2009**, *48*, 6913–6917. [[CrossRef](#)]
153. Chen, C.; Zhang, J.; Zhang, B.; Yu, C.; Peng, F.; Su, D. Revealing the enhanced catalytic activity of nitrogen-doped carbon nanotubes for oxidative dehydrogenation of propane. *Chem. Commun.* **2013**, *49*, 8151–8153. [[CrossRef](#)]
154. Dong, X.; Zhang, H.-B.; Lin, G.-D.; Yuan, Y.-Z.; Tsai, K. Highly active CNT-promoted Cu–ZnO–Al₂O₃ catalyst for methanol synthesis from H₂/CO/CO₂. *Catal. Lett.* **2003**, *85*, 237–246. [[CrossRef](#)]
155. Gopannagari, M.; Chaturvedi, H. Light induced aggregation of specific single walled carbon nanotubes. *Nanoscale* **2015**, *7*, 16590–16596. [[CrossRef](#)]
156. Karousis, N.; Tagmatarchis, N.; Tasis, D. Current progress on the chemical modification of carbon nanotubes. *Chem. Rev.* **2010**, *110*, 5366–5397. [[CrossRef](#)] [[PubMed](#)]
157. Kemnade, N.; Shearer, C.; Dieterle, D.; Cherevan, A.; Gebhardt, P.; Wilde, G.; Eder, D. Non-destructive functionalisation for atomic layer deposition of metal oxides on carbon nanotubes: Effect of linking agents and defects. *Nanoscale* **2015**, *7*, 3028–3034. [[CrossRef](#)] [[PubMed](#)]
158. Natarajan, T.S.; Lee, J.Y.; Bajaj, H.C.; Jo, W.-K.; Tayade, R.J. Synthesis of multiwall carbon nanotubes/TiO₂ nanotube composites with enhanced photocatalytic decomposition efficiency. *Catal. Today* **2017**, *282*, 13–23. [[CrossRef](#)]
159. Pawar, R.C.; Kang, S.; Ahn, S.H.; Lee, C.S. Gold nanoparticle modified graphitic carbon nitride/multi-walled carbon nanotube (gC₃N₄/CNTs/Au) hybrid photocatalysts for effective water splitting and degradation. *RSC Adv.* **2015**, *5*, 24281–24292. [[CrossRef](#)]
160. Pawar, A.S.; Garje, S.S.; Revaprasadu, N. Synthesis and characterization of CdS nanocrystallites and OMWCNT-supported cadmium sulfide composite and their photocatalytic activity under visible light irradiation. *Mater. Chem. Phys.* **2016**, *183*, 366–374. [[CrossRef](#)]
161. Shetti, N.P.; Nayak, D.S.; Kuchinad, G.T.; Naik, R.R. Electrochemical behavior of thiosalicylic acid at γ -Fe₂O₃ nanoparticles and clay composite carbon electrode. *Electrochim. Acta* **2018**, *269*, 204–211. [[CrossRef](#)]
162. Manasa, G.; Bhakta, A.K.; Mekhalif, Z.; Mascarenhas, R.J. Voltammetric study and rapid quantification of resorcinol in hair dye and biological samples using ultrasensitive maghemite/MWCNT modified carbon paste electrode. *Electroanalysis* **2019**, *31*, 1363–1372. [[CrossRef](#)]
163. Nate, Z.; Gill, A.A.S.; Shinde, S.; Chauhan, R.; Inamdar, S.N.; Karpoornath, R. A simple in-situ flame synthesis of nanocomposite (MWCNTs-Fe₂O₃) for electrochemical sensing of proguanil in pharmaceutical formulation. *Diam. Relat. Mater.* **2021**, *111*, 108178. [[CrossRef](#)]
164. Rai, S.; Ikram, A.; Sahai, S.; Dass, S.; Shrivastav, R.; Satsangi, V.R. Photoactivity of MWCNTs modified α -Fe₂O₃ photoelectrode towards efficient solar water splitting. *Renew. Energy* **2015**, *83*, 447–454. [[CrossRef](#)]
165. Hakamizadeh, M.; Afshar, S.; Tadjarodi, A.; Khajavian, R.; Fadaie, M.R.; Bozorgi, B. Improving hydrogen production via water splitting over Pt/TiO₂/activated carbon nanocomposite. *Int. J. Hydrogen Energy* **2014**, *39*, 7262–7269. [[CrossRef](#)]
166. Reddy, R.; Bhargav, U.; Shankar, M.V. Multiwalled carbon nanotubes in titania based nanocomposite as trap for photoexcitons for enhanced photocatalytic hydrogen production under solar light irradiation. *Mater. Res. Bull.* **2018**, *106*, 271–275. [[CrossRef](#)]
167. Kang, S.-Z.; Chen, L.; Li, X.; Mu, J. Composite photocatalyst containing Eosin Y and multiwalled carbon nanotubes loaded with CuO/NiO: Mixed metal oxide as an active center of H₂ evolution from water. *Appl. Surf. Sci.* **2012**, *258*, 6029–6033. [[CrossRef](#)]
168. Gopannagari, M.; Kumar, D.P.; Park, H.; Kim, E.H.; Bhavani, P.; Reddy, D.A.; Kim, T.K. Influence of surface-functionalized multi-walled carbon nanotubes on CdS nanohybrids for effective photocatalytic hydrogen production. *Appl. Catal. B Environ.* **2018**, *236*, 294–303. [[CrossRef](#)]
169. Dang, H.; Qiu, Y.; Cheng, Z.; Yang, W.; Wu, H.; Fan, H.; Dong, X. Hydrothermal preparation and characterization of nanostructured CNTs/ZnFe₂O₄ composites for solar water splitting application. *Ceram. Int.* **2016**, *42*, 10520–10525. [[CrossRef](#)]
170. Ng, B.-J.; Putri, L.K.; Tan, L.-L.; Pasbakhsh, P.; Chai, S.-P. All-solid-state Z-scheme photocatalyst with carbon nanotubes as an electron mediator for hydrogen evolution under simulated solar light. *Chem. Eng. J.* **2017**, *316*, 41–49. [[CrossRef](#)]
171. Zhang, J.; Liu, S.; Yu, J.; Jaroniec, M. A simple cation exchange approach to Bi-doped ZnS hollow spheres with enhanced UV and visible-light photocatalytic H₂-production activity. *J. Mater. Chem.* **2011**, *21*, 14655–14662. [[CrossRef](#)]
172. Subrahmanyam, M.; Supriya, V.; Reddy, P.R. Photocatalytic H₂ production with CdS-based catalysts from a sulphide/sulphite substrate: An effort to develop MgO-supported catalysts. *Int. J. Hydrogen Energy* **1996**, *21*, 99–106. [[CrossRef](#)]
173. Wu, J.-C.; Zheng, J.; Zacherl, C.L.; Wu, P.; Liu, Z.-K.; Xu, R. Hybrid Functionals Study of Band Bowing, Band Edges and Electronic Structures of Cd_{1-x}Zn_xS Solid Solution. *J. Phys. Chem. C* **2011**, *115*, 19741–19748. [[CrossRef](#)]

174. Cao, S.; Yu, J. Carbon-based H₂-production photocatalytic materials. *J. Photochem. Photobiol. C Photochem. Rev.* **2016**, *27*, 72–99. [[CrossRef](#)]
175. Yao, Z.; Wang, L.; Zhang, Y.; Yu, Z.; Jiang, Z. Carbon nanotube modified Zn_{0.83}Cd_{0.17}S nanocomposite photocatalyst and its hydrogen production under visible-light. *Int. J. Hydrogen Energy* **2014**, *39*, 15380–15386. [[CrossRef](#)]
176. Tahir, M. La-modified TiO₂/carbon nanotubes assembly nanocomposite for efficient photocatalytic hydrogen evolution from glycerol-water mixture. *Int. J. Hydrogen Energy* **2019**, *44*, 3711–3725. [[CrossRef](#)]
177. Islam, A.; Teo, S.H.; Awual, M.R.; Taufiq-Yap, Y.H. Improving the hydrogen production from water over MgO promoted Ni-Si/CNTs photocatalyst. *J. Clean. Prod.* **2019**, *238*, 117887. [[CrossRef](#)]
178. Meng, X.; Dong, Y.; Hu, Q.; Ding, Y. Co Nanoparticles Decorated with Nitrogen Doped Carbon Nanotubes for Boosting Photocatalytic Water Splitting. *ACS Sustain. Chem. Eng.* **2018**, *7*, 1753–1759. [[CrossRef](#)]
179. Rout, U.K. Prospects of India's energy and emissions for a long time frame. *Energy Policy* **2011**, *39*, 5647–5663. [[CrossRef](#)]
180. Groenewolt, M.; Antonietti, M. Synthesis of g-C₃N₄ nanoparticles in mesoporous silica host matrices. *Adv. Mater.* **2005**, *17*, 1789–1792. [[CrossRef](#)]
181. Cheng, N.; Jiang, P.; Liu, Q.; Tian, J.; Asiri, A.M.; Sun, X. Graphitic carbon nitride nanosheets: One-step, high-yield synthesis and application for Cu²⁺ detection. *Analyst* **2014**, *139*, 5065–5068. [[CrossRef](#)]
182. Hong, J.; Zhang, W.; Wang, Y.; Zhou, T.; Xu, R. Photocatalytic reduction of carbon dioxide over self-assembled carbon nitride and layered double hydroxide: The role of carbon dioxide enrichment. *ChemCatChem* **2014**, *6*, 2315–2321. [[CrossRef](#)]
183. Zhang, G.; Lan, Z.A.; Wang, X. Merging surface organometallic chemistry with graphitic carbon nitride photocatalysis for CO₂ photofixation. *ChemCatChem* **2015**, *7*, 1422–1423. [[CrossRef](#)]
184. Mao, J.; Peng, T.; Zhang, X.; Li, K.; Ye, L.; Zan, L. Effect of graphitic carbon nitride microstructures on the activity and selectivity of photocatalytic CO₂ reduction under visible light. *Catal. Sci. Technol.* **2013**, *3*, 1253–1260. [[CrossRef](#)]
185. Zhang, X.; Xie, X.; Wang, H.; Zhang, J.; Pan, B.; Xie, Y. Enhanced photoresponsive ultrathin graphitic-phase C₃N₄ nanosheets for bioimaging. *J. Am. Chem. Soc.* **2013**, *135*, 18–21. [[CrossRef](#)]
186. Zheng, Y.; Liu, J.; Liang, J.; Jaroniec, M.; Qiao, S.Z. Graphitic carbon nitride materials: Controllable synthesis and applications in fuel cells and photocatalysis. *Energy Environ. Sci.* **2012**, *5*, 6717–6731. [[CrossRef](#)]
187. Zhu, J.; Xiao, P.; Li, H.; Carabineiro, S.A. Graphitic carbon nitride: Synthesis, properties, and applications in catalysis. *ACS Appl. Mater. Interfaces* **2014**, *6*, 16449–16465. [[CrossRef](#)] [[PubMed](#)]
188. Zhao, Z.; Sun, Y.; Dong, F. Graphitic carbon nitride based nanocomposites: A review. *Nanoscale* **2015**, *7*, 15–37. [[CrossRef](#)] [[PubMed](#)]
189. Su, Q.; Sun, J.; Wang, J.; Yang, Z.; Cheng, W.; Zhang, S. Urea-derived graphitic carbon nitride as an efficient heterogeneous catalyst for CO₂ conversion into cyclic carbonates. *Catal. Sci. Technol.* **2014**, *4*, 1556–1562. [[CrossRef](#)]
190. Wang, S.; Lin, J.; Wang, X. Semiconductor–redox catalysis promoted by metal–organic frameworks for CO₂ reduction. *Phys. Chem. Chem. Phys.* **2014**, *16*, 14656–14660. [[CrossRef](#)]
191. Li, Y.; Zhou, M.; Cheng, B.; Shao, Y. Recent advances in g-C₃N₄-based heterojunction photocatalysts. *J. Mater. Sci. Technol.* **2020**, *56*, 1–17. [[CrossRef](#)]
192. Hayat, A.; Al-Sehemi, A.G.; El-Nasser, K.S.; Taha, T.A. Graphitic carbon nitride (g-C₃N₄)-based semiconductor as a beneficial candidate in photocatalysis diversity. *Int. J. Hydrogen Energy* **2022**, *47*, 5142–5191. [[CrossRef](#)]
193. Kundu, A.; Sharma, S.; Basu, S. Modulated BiOCl nanoplates with porous g-C₃N₄ nanosheets for photocatalytic degradation of color/colorless pollutants in natural sunlight. *J. Phys. Chem. Solids* **2021**, *154*, 110064. [[CrossRef](#)]
194. Singla, S.; Sharma, S.; Basu, S.; Shetti, N.P.; Reddy, K.R. Graphene/graphitic carbon nitride-based ternary nanohybrids: Synthesis methods, properties, and applications for photocatalytic hydrogen production. *FlatChem* **2020**, *24*, 100200. [[CrossRef](#)]
195. Mishra, A.; Mehta, A.; Kainth, S.; Basu, S. A comparative study on the effect of different precursors for synthesis and efficient photocatalytic activity of g-C₃N₄/TiO₂/bentonite nanocomposites. *J. Mater. Sci.* **2018**, *53*, 13126–13142. [[CrossRef](#)]
196. Qin, J.; Huo, J.; Zhang, P.; Zeng, J.; Wang, T.; Zeng, H. Improving the photocatalytic hydrogen production of Ag/g-C₃N₄ nanocomposites by dye-sensitization under visible light irradiation. *Nanoscale* **2016**, *8*, 2249–2259. [[CrossRef](#)] [[PubMed](#)]
197. Zeng, J.; Song, T.; Lv, M.; Wang, T.; Qin, J.; Zeng, H. Plasmonic photocatalyst Au/g-C₃N₄/NiFe₂O₄ nanocomposites for enhanced visible-light-driven photocatalytic hydrogen evolution. *RSC Adv.* **2016**, *6*, 54964–54975. [[CrossRef](#)]
198. Zhang, P.; Wang, T.; Zeng, H. Design of Cu-Cu₂O/g-C₃N₄ nanocomponent photocatalysts for hydrogen evolution under visible light irradiation using water-soluble Erythrosin B dye sensitization. *Appl. Surf. Sci.* **2017**, *391*, 404–414. [[CrossRef](#)]
199. Jiang, D.; Zhang, Y.; Chu, H.; Liu, J.; Wan, J.; Chen, M. N-doped graphene quantum dots as an effective photocatalyst for the photochemical synthesis of silver deposited porous graphitic C₃N₄ nanocomposites for nonenzymatic electrochemical H₂O₂ sensing. *RSC Adv.* **2014**, *4*, 16163–16171. [[CrossRef](#)]
200. Wang, W.; Jimmy, C.Y.; Shen, Z.; Chan, D.K.; Gu, T. g-C₃N₄ quantum dots: Direct synthesis, upconversion properties and photocatalytic application. *Chem. Commun.* **2014**, *50*, 10148–10150. [[CrossRef](#)]
201. Patnaik, S.; Martha, S.; Parida, K. An overview of the structural, textural and morphological modulations of g-C₃N₄ towards photocatalytic hydrogen production. *RSC Adv.* **2016**, *6*, 46929–46951. [[CrossRef](#)]
202. Wang, X.; Maeda, K.; Thomas, A.; Takanabe, K.; Xin, G.; Carlsson, J.M.; Domen, K.; Antonietti, M. A metal-free polymeric photocatalyst for hydrogen production from water under visible light. *Nat. Mater.* **2009**, *8*, 76–80. [[CrossRef](#)]

203. Liu, W.; Liu, G.; Shi, N.; Liu, D.; Wen, F. Carbon Quantum Dot-Modified and Chloride-Doped Ordered Macroporous Graphitic Carbon Nitride Composites for Hydrogen Evolution. *ACS Appl. Nano Mater.* **2020**, *3*, 12188–12197. [CrossRef]
204. Gao, Q.; Xu, J.; Wang, Z.; Zhu, Y. Enhanced visible photocatalytic oxidation activity of perylene diimide/g-C₃N₄ nn heterojunction via π - π interaction and interfacial charge separation. *Appl. Catal. B Environ.* **2020**, *271*, 118933. [CrossRef]
205. Kumar, A.; Khan, M.; He, J.; Lo, I.M. Visible-light-driven magnetically recyclable terephthalic acid functionalized g-C₃N₄/TiO₂ heterojunction nanophotocatalyst for enhanced degradation of PPCPs. *Appl. Catal. B Environ.* **2020**, *270*, 118898. [CrossRef]
206. Li, H.; Wang, L.; Liu, Y.; Lei, J.; Zhang, J. Mesoporous graphitic carbon nitride materials: Synthesis and modifications. *Res. Chem. Intermed.* **2016**, *42*, 3979–3998. [CrossRef]
207. Jiang, L.; Yuan, X.; Pan, Y.; Liang, J.; Zeng, G.; Wu, Z.; Wang, H. Doping of graphitic carbon nitride for photocatalysis: A review. *Appl. Catal. B Environ.* **2017**, *217*, 388–406. [CrossRef]
208. Ong, W.-J. 2D/2D graphitic carbon nitride (g-C₃N₄) heterojunction nanocomposites for photocatalysis: Why does face-to-face interface matter? *Front. Mater.* **2017**, *4*, 11. [CrossRef]
209. Fu, J.; Yu, J.; Jiang, C.; Cheng, B. g-C₃N₄-Based heterostructured photocatalysts. *Adv. Energy Mater.* **2018**, *8*, 1701503. [CrossRef]
210. Yin, S.; Han, J.; Zhou, T.; Xu, R. Recent progress in g-C₃N₄ based low cost photocatalytic system: Activity enhancement and emerging applications. *Catal. Sci. Technol.* **2015**, *5*, 5048–5061. [CrossRef]
211. Zhu, Z.; Tang, X.; Ma, C.; Song, M.; Gao, N.; Wang, Y.; Huo, P.; Lu, Z.; Yan, Y. Fabrication of conductive and high-dispersed Ppy@Ag/g-C₃N₄ composite photocatalysts for removing various pollutants in water. *Appl. Surf. Sci.* **2016**, *387*, 366–374. [CrossRef]
212. Guo, Y.; Li, J.; Gao, Z.; Zhu, X.; Liu, Y.; Wei, Z.; Zhao, W.; Sun, C. A simple and effective method for fabricating novel p-n heterojunction photocatalyst g-C₃N₄/Bi₄Ti₃O₁₂ and its photocatalytic performances. *Appl. Catal. B Environ.* **2016**, *192*, 57–71. [CrossRef]
213. Huu, H.T.; Thi, M.D.N.; Nguyen, V.P.; Thi, L.N.; Phan, T.T.T.; Hoang, Q.D.; Luc, H.H.; Kim, S.J.; Vo, V. One-pot synthesis of S-scheme MoS₂/g-C₃N₄ heterojunction as effective visible light photocatalyst. *Sci. Rep.* **2021**, *11*, 14787.
214. Zhang, H. Ultrathin two-dimensional nanomaterials. *ACS Nano* **2015**, *9*, 9451–9469. [CrossRef]
215. Lu, X.; Jin, Y.; Zhang, X.; Xu, G.; Wang, D.; Lv, J.; Zheng, Z.; Wu, Y. Controllable synthesis of graphitic C₃N₄/ultrathin MoS₂ nanosheet hybrid nanostructures with enhanced photocatalytic performance. *Dalton Trans.* **2016**, *45*, 15406–15414. [CrossRef]
216. Sundaram, I.M.; Kalimuthu, S.; Sekar, K.; Rajendran, S. Hierarchical TiO₂ spheroids decorated g-C₃N₄ nanocomposite for solar driven hydrogen production and water depollution. *Int. J. Hydrogen Energy* **2022**, *47*, 3709–3721. [CrossRef]
217. Beyhaqi, A.; Azimi, S.M.T.; Chen, Z.; Hu, C.; Zeng, Q. Exfoliated and plicated g-C₃N₄ nanosheets for efficient photocatalytic organic degradation and hydrogen evolution. *Int. J. Hydrogen Energy* **2021**, *46*, 20547–20559. [CrossRef]
218. Chen, T.; Quan, W.; Yu, L.; Hong, Y.; Song, C.; Fan, M.; Xiao, L.; Gu, W.; Shi, W. One-step synthesis and visible-light-driven H₂ production from water splitting of Ag quantum dots/g-C₃N₄ photocatalysts. *J. Alloys Compd.* **2016**, *686*, 628–634. [CrossRef]
219. Sun, Y.; Xiong, T.; Ni, Z.; Liu, J.; Dong, F.; Zhang, W.; Ho, W.-K. Improving g-C₃N₄ photocatalysis for NO_x removal by Ag nanoparticles decoration. *Appl. Surf. Sci.* **2015**, *358*, 356–362. [CrossRef]
220. Wu, H.; Chen, Z.; Wang, Y.; Cao, E.; Xiao, F.; Chen, S.; Du, S.; Wu, Y.; Ren, Z. Regulating the allocation of N and P in codoped graphene via supramolecular control to remarkably boost hydrogen evolution. *Energy Environ. Sci.* **2019**, *12*, 2697–2705. [CrossRef]
221. Che, W.; Cheng, W.; Yao, T.; Tang, F.; Liu, W.; Su, H.; Huang, Y.; Liu, Q.; Liu, J.; Hu, F. Fast photoelectron transfer in (Cring)-C₃N₄ plane heterostructural nanosheets for overall water splitting. *J. Am. Chem. Soc.* **2017**, *139*, 3021–3026. [CrossRef]
222. Qi, L.; Yu, J.; Jaroniec, M. Preparation and enhanced visible-light photocatalytic H₂-production activity of CdS-sensitized Pt/TiO₂ nanosheets with exposed (001) facets. *Phys. Chem. Chem. Phys.* **2011**, *13*, 8915–8923. [CrossRef]
223. Han, X.; Yuan, A.; Yao, C.; Xi, F.; Liu, J.; Dong, X. Synergistic effects of phosphorous/sulfur co-doping and morphological regulation for enhanced photocatalytic performance of graphitic carbon nitride nanosheets. *J. Mater. Sci.* **2019**, *54*, 1593–1605. [CrossRef]
224. Wang, Y.; Li, H.; Yao, J.; Wang, X.; Antonietti, M. Synthesis of boron doped polymeric carbon nitride solids and their use as metal-free catalysts for aliphatic C-H bond oxidation. *Chem. Sci.* **2011**, *2*, 446–450. [CrossRef]
225. Zou, J.; Yu, Y.; Yan, W.; Meng, J.; Zhang, S.; Wang, J. A facile route to synthesize boron-doped g-C₃N₄ nanosheets with enhanced visible-light photocatalytic activity. *J. Mater. Sci.* **2019**, *54*, 6867–6881. [CrossRef]
226. Thaweesak, S.; Wang, S.; Lyu, M.; Xiao, M.; Peerakiathajohn, P.; Wang, L. Boron-doped graphitic carbon nitride nanosheets for enhanced visible light photocatalytic water splitting. *Dalton Trans.* **2017**, *46*, 10714–10720. [CrossRef] [PubMed]
227. Yu, J.; Xu, C.; Tian, Z.; Lin, Y.; Shi, Z. Facilely synthesized N-doped carbon quantum dots with high fluorescent yield for sensing Fe³⁺. *New J. Chem.* **2016**, *40*, 2083–2088. [CrossRef]
228. Sun, Y.; Zhang, Z.; Xie, A.; Xiao, C.; Li, S.; Huang, F.; Shen, Y. An ordered and porous N-doped carbon dot-sensitized Bi₂O₃ inverse opal with enhanced photoelectrochemical performance and photocatalytic activity. *Nanoscale* **2015**, *7*, 13974–13980. [CrossRef]
229. Gholami, T.; Salavati-Niasari, M.; Varshoy, S. Electrochemical hydrogen storage capacity and optical properties of NiAl₂O₄/NiO nanocomposite synthesized by green method. *Int. J. Hydrogen Energy* **2017**, *42*, 5235–5245. [CrossRef]
230. Zhao, H.; Zhang, H.; Cui, G.; Dong, Y.; Wang, G.; Jiang, P.; Wu, X.; Zhao, N. A photochemical synthesis route to typical transition metal sulfides as highly efficient cocatalyst for hydrogen evolution: From the case of NiS/g-C₃N₄. *Appl. Catal. B Environ.* **2018**, *225*, 284–290. [CrossRef]

231. He, H.; Cao, J.; Guo, M.; Lin, H.; Zhang, J.; Chen, Y.; Chen, S. Distinctive ternary CdS/Ni₂P/g-C₃N₄ composite for overall water splitting: Ni₂P accelerating separation of photocarriers. *Appl. Catal. B Environ.* **2019**, *249*, 246–256. [CrossRef]
232. Wulan, B.-R.; Yi, S.-S.; Li, S.-J.; Duan, Y.-X.; Yan, J.-M.; Jiang, Q. Amorphous nickel pyrophosphate modified graphitic carbon nitride: An efficient photocatalyst for hydrogen generation from water splitting. *Appl. Catal. B Environ.* **2018**, *231*, 43–50. [CrossRef]
233. Deng, P.; Hong, W.; Cheng, Z.; Zhang, L.; Hou, Y. Facile fabrication of nickel/porous g-C₃N₄ by using carbon dot as template for enhanced photocatalytic hydrogen production. *Int. J. Hydrogen Energy* **2020**, *45*, 33543–33551. [CrossRef]
234. Xi, G.; Ye, J.; Ma, Q.; Su, N.; Bai, H.; Wang, C. In situ growth of metal particles on 3D urchin-like WO₃ nanostructures. *J. Am. Chem. Soc.* **2012**, *134*, 6508–6511. [CrossRef]
235. Yu, J.; Qi, L.; Cheng, B.; Zhao, X. Effect of calcination temperatures on microstructures and photocatalytic activity of tungsten trioxide hollow microspheres. *J. Hazard. Mater.* **2008**, *160*, 621–628. [CrossRef]
236. Cao, B.; Chen, J.; Tang, X.; Zhou, W. Growth of monoclinic WO₃ nanowire array for highly sensitive NO₂ detection. *J. Mater. Chem.* **2009**, *19*, 2323–2327. [CrossRef]
237. Kondrachova, L.V.; May, R.A.; Cone, C.W.; Vanden Bout, D.A.; Stevenson, K.J. Evaluation of lithium ion insertion reactivity via electrochromic diffraction-based imaging. *Langmuir* **2009**, *25*, 2508–2518. [CrossRef] [PubMed]
238. Chen, S.; Hu, Y.; Meng, S.; Fu, X. Study on the separation mechanisms of photogenerated electrons and holes for composite photocatalysts g-C₃N₄-WO₃. *Appl. Catal. B Environ.* **2014**, *150*, 564–573. [CrossRef]
239. Sun, X.-Y.; Zhang, F.-J.; Kong, C. Porous g-C₃N₄/WO₃ photocatalyst prepared by simple calcination for efficient hydrogen generation under visible light. *Colloids Surf. A Physicochem. Eng. Asp.* **2020**, *594*, 124653. [CrossRef]
240. He, K.; Xie, J.; Luo, X.; Wen, J.; Ma, S.; Li, X.; Fang, Y.; Zhang, X. Enhanced visible light photocatalytic H₂ production over Z-scheme g-C₃N₄ nanosheets/WO₃ nanorods nanocomposites loaded with Ni(OH)_x cocatalysts. *Chin. J. Catal.* **2017**, *38*, 240–252. [CrossRef]
241. Cheng, C.; Shi, J.; Hu, Y.; Guo, L. WO₃/g-C₃N₄ composites: One-pot preparation and enhanced photocatalytic H₂ production under visible-light irradiation. *Nanotechnology* **2017**, *28*, 164002. [CrossRef]
242. Han, X.; Xu, D.; An, L.; Hou, C.; Li, Y.; Zhang, Q.; Wang, H. WO₃/g-C₃N₄ two-dimensional composites for visible-light driven photocatalytic hydrogen production. *Int. J. Hydrogen Energy* **2018**, *43*, 4845–4855. [CrossRef]
243. Su, L.-X.; Huang, Q.-Z.; Lou, Q.; Liu, Z.-Y.; Sun, J.-L.; Zhang, Z.-T.; Qin, S.-R.; Li, X.; Zang, J.-H.; Dong, L. Effective light scattering and charge separation in nanodiamond@ g-C₃N₄ for enhanced visible-light hydrogen evolution. *Carbon* **2018**, *139*, 164–171. [CrossRef]
244. Su, L.-X.; Liu, Z.-Y.; Ye, Y.-L.; Shen, C.-L.; Lou, Q.; Shan, C.-X. Heterostructured boron doped nanodiamonds@ g-C₃N₄ nanocomposites with enhanced photocatalytic capability under visible light irradiation. *Int. J. Hydrogen Energy* **2019**, *44*, 19805–19815. [CrossRef]
245. Shen, R.; He, K.; Zhang, A.; Li, N.; Ng, Y.H.; Zhang, P.; Hu, J.; Li, X. In-situ construction of metallic Ni₃C@Ni core-shell cocatalysts over g-C₃N₄ nanosheets for shell-thickness-dependent photocatalytic H₂ production. *Appl. Catal. B Environ.* **2021**, *291*, 120104. [CrossRef]
246. Sun, M.; Zhou, Y.; Yu, T.; Wang, J. Synthesis of g-C₃N₄/WO₃-carbon microsphere composites for photocatalytic hydrogen production. *Int. J. Hydrogen Energy* **2022**, *47*, 10261–10276. [CrossRef]
247. Curl, R.F.; Smalley, R.E. Probing C₆₀. *Science* **1988**, *242*, 1017–1022. [CrossRef] [PubMed]
248. Xu, T.; Shen, W.; Huang, W.; Lu, X. Fullerene micro/nanostructures: Controlled synthesis and energy applications. *Mater. Today Nano* **2020**, *11*, 100081. [CrossRef]
249. Park, C.; Yoon, E.; Kawano, M.; Joo, T.; Choi, H.C. Self-crystallization of C₇₀ cubes and remarkable enhancement of photoluminescence. *Angew. Chem.* **2010**, *122*, 9864–9869. [CrossRef]
250. Hale, P.D. Discrete-variational-X. alpha. electronic structure studies of the spherical C₆₀ cluster: Prediction of ionization potential and electronic transition energy. *J. Am. Chem. Soc.* **1986**, *108*, 6087–6088. [CrossRef]
251. Nimibofa, A.; Newton, E.A.; Cyprain, A.Y.; Donbebe, W. Fullerenes: Synthesis and applications. *J. Mater. Sci.* **2018**, *7*, 22–33. [CrossRef]
252. Li, C.-Z.; Yip, H.-L.; Jen, A.K.-Y. Functional fullerenes for organic photovoltaics. *J. Mater. Chem.* **2012**, *22*, 4161–4177. [CrossRef]
253. Dugan, L.; Lovett, E.; Quick, K.; Lotharius, J.; Lin, T.; O'malley, K. Fullerene-based antioxidants and neurodegenerative disorders. *Park. Relat. Disord.* **2001**, *7*, 243–246. [CrossRef]
254. Song, X.; Gasparini, N.; Baran, D. The Influence of Solvent Additive on Polymer Solar Cells Employing Fullerene and Non-Fullerene Acceptors. *Adv. Electron. Mater.* **2018**, *4*, 1700358. [CrossRef]
255. Lopez-Andarias, J.; Frontera, A.; Matile, S. Anion-π catalysis on fullerenes. *J. Am. Chem. Soc.* **2017**, *139*, 13296–13299. [CrossRef]
256. Youssef, Z.; Colombeau, L.; Yesmurzayeva, N.; Baros, F.; Vanderesse, R.; Hamieh, T.; Toufaily, J.; Frochot, C.; Roques-Carnes, T.; Acherar, S. Dye-sensitized nanoparticles for heterogeneous photocatalysis: Cases studies with TiO₂, ZnO, fullerene and graphene for water purification. *Dye. Pigment.* **2018**, *159*, 49–71. [CrossRef]
257. Bhakta, P.; Barthunia, B. Fullerene and its applications: A review. *J. Indian Acad. Oral Med. Radiol.* **2020**, *32*, 159. [CrossRef]
258. Ordaz, J.C.; Anota, E.C.; Villanueva, M.S.; Castro, M. Possibility of a magnetic [BN fullerene: B 6 cluster]—Nanocomposite as a vehicle for the delivery of dapsone. *New J. Chem.* **2017**, *41*, 8045–8052. [CrossRef]

259. Bai, X.; Wang, L.; Wang, Y.; Yao, W.; Zhu, Y. Enhanced oxidation ability of g-C₃N₄ photocatalyst via C60 modification. *Appl. Catal. B Environ.* **2014**, *152*, 262–270. [CrossRef]
260. Pan, Y.; Liu, X.; Zhang, W.; Liu, Z.; Zeng, G.; Shao, B.; Liang, Q.; He, Q.; Yuan, X.; Huang, D.; et al. Advances in photocatalysis based on fullerene C60 and its derivatives: Properties, mechanism, synthesis, and applications. *Appl. Catal. B Environ.* **2020**, *265*, 118579. [CrossRef]
261. Abe, T.; Chiba, J.; Ishidoya, M.; Nagai, K. Organophotocatalysis system of p/n bilayers for wide visible-light-induced molecular hydrogen evolution. *RSC Adv.* **2012**, *2*, 7992–7996. [CrossRef]
262. Guan, J.; Wu, J.; Jiang, D.; Zhu, X.; Guan, R.; Lei, X.; Du, P.; Zeng, H.; Yang, S. Hybridizing MoS₂ and C60 via a van der Waals heterostructure toward synergistically enhanced visible light photocatalytic hydrogen production activity. *Int. J. Hydrogen Energy* **2018**, *43*, 8698–8706. [CrossRef]
263. Moor, K.J.; Valle, D.C.; Li, C.; Kim, J.-H. Improving the visible light photoactivity of supported fullerene photocatalysts through the use of [C70] fullerene. *Environ. Sci. Technol.* **2015**, *49*, 6190–6197. [CrossRef]
264. Yao, S.; Yuan, X.; Jiang, L.; Xiong, T.; Zhang, J. Recent Progress on Fullerene-Based Materials: Synthesis, Properties, Modifications, and Photocatalytic Applications. *Materials* **2020**, *13*, 2924. [CrossRef]
265. Bilal Tahir, M.; Nabi, G.; Rafique, M.; Khalid, N. Role of fullerene to improve the WO₃ performance for photocatalytic applications and hydrogen evolution. *Int. J. Energy Res.* **2018**, *42*, 4783–4789. [CrossRef]
266. Shahzad, K.; Tahir, M.B.; Sagir, M. Engineering the performance of heterogeneous WO₃/fullerene@Ni₃B/Ni(OH)₂ photocatalysts for hydrogen generation. *Int. J. Hydrogen Energy* **2019**, *44*, 21738–21745. [CrossRef]
267. Song, T.; Zhang, P.; Zeng, J.; Wang, T.; Ali, A.; Zeng, H. Boosting the photocatalytic H₂ evolution activity of Fe₂O₃ polymorphs (α -, γ - and β -Fe₂O₃) by fullerene [C 60]-modification and dye-sensitization under visible light irradiation. *RSC Adv.* **2017**, *7*, 29184–29192. [CrossRef]
268. Yao, W.; Huang, C.; Muradov, N.; Ali, T. A novel Pd–Cr₂O₃/CdS photocatalyst for solar hydrogen production using a regenerable sacrificial donor. *Int. J. Hydrogen Energy* **2011**, *36*, 4710–4715. [CrossRef]
269. Trenczek-Zajac, A.; Radecka, M.; Jasinski, M.; Michalow, K.; Rekas, M.; Kusior, E.; Zakrzewska, K.; Heel, A.; Graule, T.; Kowalski, K. Influence of Cr on structural and optical properties of TiO₂: Cr nanopowders prepared by flame spray synthesis. *J. Power Sources* **2009**, *194*, 104–111. [CrossRef]
270. Song, T.; Huo, J.; Liao, T.; Zeng, J.; Qin, J.; Zeng, H. Fullerene [C60] modified Cr_{2-x}Fe_xO₃ nanocomposites for enhanced photocatalytic activity under visible light irradiation. *Chem. Eng. J.* **2016**, *287*, 359–366. [CrossRef]
271. Cai, Q.; Hu, Z.; Zhang, Q.; Li, B.; Shen, Z. Fullerene (C60)/CdS nanocomposite with enhanced photocatalytic activity and stability. *Appl. Surf. Sci.* **2017**, *403*, 151–158. [CrossRef]
272. Hou, J.; Lan, X.; Shi, J.; Yu, S.; Zhang, Y.; Wang, H.; Ren, C. A mild and simple method to fabricate commercial TiO₂ (P25) and C60 composite for highly enhancing H₂ generation. *Int. J. Hydrogen Energy* **2020**, *45*, 2852–2861. [CrossRef]
273. Song, S.; Meng, A.; Jiang, S.; Cheng, B. Three-dimensional hollow graphene efficiently promotes electron transfer of Ag₃PO₄ for photocatalytically eliminating phenol. *Appl. Surf. Sci.* **2018**, *442*, 224–231. [CrossRef]
274. Wang, J.; Ng, Y.H.; Lim, Y.-F.; Ho, G.W. Vegetable-extracted carbon dots and their nanocomposites for enhanced photocatalytic H₂ production. *RSC Adv.* **2014**, *4*, 44117–44123. [CrossRef]
275. Guo, Y.; Yao, P.; Zhu, D.; Gu, C. A novel method for the development of a carbon quantum dot/carbon nitride hybrid photocatalyst that responds to infrared light irradiation. *J. Mater. Chem. A* **2015**, *3*, 13189–13192. [CrossRef]
276. Qin, J.; Zeng, H. Photocatalysts fabricated by depositing plasmonic Ag nanoparticles on carbon quantum dots/graphitic carbon nitride for broad spectrum photocatalytic hydrogen generation. *Appl. Catal. B Environ.* **2017**, *209*, 161–173. [CrossRef]
277. Bruchez, M., Jr.; Moronne, M.; Gin, P.; Weiss, S.; Alivisatos, A.P. Semiconductor nanocrystals as fluorescent biological labels. *Science* **1998**, *281*, 2013–2016. [CrossRef] [PubMed]
278. Wang, Y.; Zhu, Y.; Yu, S.; Jiang, C. Fluorescent carbon dots: Rational synthesis, tunable optical properties and analytical applications. *RSC Adv.* **2017**, *7*, 40973–40989. [CrossRef]
279. Yao, Y.; Zhang, H.; Hu, K.; Nie, G.; Yang, Y.; Wang, Y.; Duan, X.; Wang, S. Carbon dots based photocatalysis for environmental applications. *J. Environ. Chem. Eng.* **2022**, *10*, 107336. [CrossRef]
280. Meng, X.-B.; Sheng, J.-L.; Tang, H.-L.; Sun, X.-J.; Dong, H.; Zhang, F.-M. Metal-organic framework as nanoreactors to co-incorporate carbon nanodots and CdS quantum dots into the pores for improved H₂ evolution without noble-metal cocatalyst. *Appl. Catal. B Environ.* **2019**, *244*, 340–346. [CrossRef]
281. Yu, H.; Zhao, Y.; Zhou, C.; Shang, L.; Peng, Y.; Cao, Y.; Wu, L.; Tung, C.-H.; Zhang, T. Carbon quantum dots/TiO₂ composites for efficient photocatalytic hydrogen evolution. *J. Mater. Chem. A* **2014**, *2*, 3344–3351. [CrossRef]
282. Wang, Y.; Shi, R.; Lin, J.; Zhu, Y. Enhancement of photocurrent and photocatalytic activity of ZnO hybridized with graphite-like C₃N₄. *Energy Environ. Sci.* **2011**, *4*, 2922–2929. [CrossRef]
283. Zhao, L.; Chen, X.; Wang, X.; Zhang, Y.; Wei, W.; Sun, Y.; Antonietti, M.; Titirici, M.-M. One-step solvothermal synthesis of a carbon@TiO₂ dyade structure effectively promoting visible-light photocatalysis. *Adv. Mater.* **2010**, *22*, 3317. [CrossRef]
284. Zhang, P.; Song, T.; Wang, T.; Zeng, H. In-situ synthesis of Cu nanoparticles hybridized with carbon quantum dots as a broad spectrum photocatalyst for improvement of photocatalytic H₂ evolution. *Appl. Catal. B Environ.* **2017**, *206*, 328–335. [CrossRef]
285. Pirsaeheb, M.; Asadi, A.; Sillanpää, M.; Farhadian, N. Application of carbon quantum dots to increase the activity of conventional photocatalysts: A systematic review. *J. Mol. Liq.* **2018**, *271*, 857–871. [CrossRef]

286. Wang, Y.; Liu, X.; Liu, J.; Han, B.; Hu, X.; Yang, F.; Xu, Z.; Li, Y.; Li, Z.; Zhao, Y. Carbon Quantum Dot Implanted Graphite Carbon Nitride Nanotubes: Excellent Charge Separation and Enhanced Photocatalytic Hydrogen Evolution. *Angew. Chem. Int. Ed. Engl.* **2018**, *57*, 5765–5771. [[CrossRef](#)] [[PubMed](#)]
287. Huang, Y.; Liang, Y.; Rao, Y.; Zhu, D.; Cao, J.; Shen, Z.; Ho, W.; Lee, S.C. Environment-Friendly Carbon Quantum Dots/ZnFe₂O₄ Photocatalysts: Characterization, Biocompatibility, and Mechanisms for NO Removal. *Environ. Sci. Technol.* **2017**, *51*, 2924–2933. [[CrossRef](#)] [[PubMed](#)]
288. Nie, H.; Liu, Y.; Li, Y.; Wei, K.; Wu, Z.; Shi, H.; Huang, H.; Liu, Y.; Shao, M.; Kang, Z. In-situ transient photovoltage study on interface electron transfer regulation of carbon dots/NiCo₂O₄ photocatalyst for the enhanced overall water splitting activity. *Nano Res.* **2022**, *15*, 1786–1795. [[CrossRef](#)]
289. Luo, H.; Liu, Y.; Dimitrov, S.D.; Steier, L.; Guo, S.; Li, X.; Feng, J.; Xie, F.; Fang, Y.; Sapelkin, A. Pt single-atoms supported on nitrogen-doped carbon dots for highly efficient photocatalytic hydrogen generation. *J. Mater. Chem. A* **2020**, *8*, 14690–14696. [[CrossRef](#)]
290. Yu, Z.; Meng, J.; Li, Y.; Li, Y. Efficient photocatalytic hydrogen production from water over a CuO and carbon fiber comodified TiO₂ nanocomposite photocatalyst. *Int. J. Hydrogen Energy* **2013**, *38*, 16649–16655. [[CrossRef](#)]
291. Lian, Z.; Xu, P.; Wang, W.; Zhang, D.; Xiao, S.; Li, X.; Li, G. C60-decorated CdS/TiO₂ mesoporous architectures with enhanced photostability and photocatalytic activity for H₂ evolution. *ACS Appl. Mater. Interfaces* **2015**, *7*, 4533–4540. [[CrossRef](#)]
292. Nguyen, B.S.; Xiao, Y.K.; Shih, C.Y.; Nguyen, V.C.; Chou, W.Y.; Teng, H. Electronic structure manipulation of graphene dots for effective hydrogen evolution from photocatalytic water decomposition. *Nanoscale* **2018**, *10*, 10721–10730. [[CrossRef](#)]
293. Kwon, K.C.; Choi, K.S.; Kim, C.; Kim, S.Y. Role of Metal Cations in Alkali Metal Chloride Doped Graphene. *J. Phys. Chem. C* **2014**, *118*, 8187–8193. [[CrossRef](#)]
294. Putri, L.K.; Ng, B.J.; Ong, W.J.; Lee, H.W.; Chang, W.S.; Chai, S.P. Heteroatom Nitrogen- and Boron-Doping as a Facile Strategy to Improve Photocatalytic Activity of Standalone Reduced Graphene Oxide in Hydrogen Evolution. *ACS Appl. Mater. Interfaces* **2017**, *9*, 4558–4569. [[CrossRef](#)]
295. Latorre-Sanchez, M.; Primo, A.; Garcia, H. P-doped graphene obtained by pyrolysis of modified alginate as a photocatalyst for hydrogen generation from water-methanol mixtures. *Angew. Chem. Int. Ed. Engl.* **2013**, *52*, 11813–11816. [[CrossRef](#)]
296. Huang, T.; Xu, Z.; Zeng, G.; Zhang, P.; Song, T.; Wang, Y.; Wang, T.; Huang, S.; Wang, T.; Zeng, H. Selective deposition of plasmonic copper on few layers graphene with specific defects for efficiently synchronous photocatalytic hydrogen production. *Carbon* **2019**, *143*, 257–267. [[CrossRef](#)]
297. Maarisetty, D.; Baral, S.S. Defect engineering in photocatalysis: Formation, chemistry, optoelectronics, and interface studies. *J. Mater. Chem. A* **2020**, *8*, 18560–18604. [[CrossRef](#)]
298. Kong, X.; Gao, P.; Jiang, R.; Feng, J.; Yang, P.; Gai, S.; Chen, Y.; Chi, Q.; Xu, F.; Ye, W. Orderly layer-by-layered TiO₂/carbon superstructures based on MXene's defect engineering for efficient hydrogen evolution. *Appl. Catal. A Gen.* **2020**, *590*, 117341. [[CrossRef](#)]
299. Hu, L.; Liao, Y.; Xia, D.; Peng, F.; Tan, L.; Hu, S.; Zheng, C.; Lu, X.; He, C.; Shu, D. Engineered photocatalytic fuel cell with oxygen vacancies-rich rGO/BiO_{1-x}I as photoanode and biomass-derived N-doped carbon as cathode: Promotion of reactive oxygen species production via Fe²⁺/Fe³⁺ redox. *Chem. Eng. J.* **2020**, *385*, 123824. [[CrossRef](#)]
300. Chen, H.; Gu, Z.-G.; Mirza, S.; Zhang, S.-H.; Zhang, J. Hollow Cu-TiO₂/C nanospheres derived from a Ti precursor encapsulated MOF coating for efficient photocatalytic hydrogen evolution. *J. Mater. Chem. A* **2018**, *6*, 7175–7181. [[CrossRef](#)]
301. Xiong, Y.; Gu, D.; Deng, X.; Tüysüz, H.; van Gestel, M.; Schüth, F.; Marlow, F. High surface area black TiO₂ templated from ordered mesoporous carbon for solar driven hydrogen evolution. *Microporous Mesoporous Mater.* **2018**, *268*, 162–169. [[CrossRef](#)]
302. Han, M.; Zhu, S.; Lu, S.; Song, Y.; Feng, T.; Tao, S.; Liu, J.; Yang, B. Recent progress on the photocatalysis of carbon dots: Classification, mechanism and applications. *Nano Today* **2018**, *19*, 201–218. [[CrossRef](#)]
303. Kandi, D.; Martha, S.; Parida, K.M. Quantum dots as enhancer in photocatalytic hydrogen evolution: A review. *Int. J. Hydrogen Energy* **2017**, *42*, 9467–9481. [[CrossRef](#)]
304. Zhao, H.; Weng, C.-C.; Ren, J.-T.; Ge, L.; Liu, Y.-P.; Yuan, Z.-Y. Phosphonate-derived nitrogen-doped cobalt phosphate/carbon nanotube hybrids as highly active oxygen reduction reaction electrocatalysts. *Chin. J. Catal.* **2020**, *41*, 259–267. [[CrossRef](#)]
305. Sun, X.; Habibur, N.; Du, H. Co_{0.85}Se magnetic nanoparticles supported on carbon nanotubes as catalyst for hydrogen evolution reaction. *Chin. J. Catal.* **2021**, *42*, 235–243. [[CrossRef](#)]
306. Li, Z.; Zhou, W.; Tang, Y.; Tan, X.; Zhang, Y.; Geng, Z.; Guo, Y.; Liu, L.; Yu, T.; Ye, J. Insights into the Operation of Noble-Metal-Free Cocatalyst 1T-WS₂-Decorated Zn_{0.5}Cd_{0.5}S for Enhanced Photocatalytic Hydrogen Evolution. *ChemSusChem* **2021**, *14*, 4752–4763. [[CrossRef](#)]

Disclaimer/Publisher's Note: The statements, opinions and data contained in all publications are solely those of the individual author(s) and contributor(s) and not of MDPI and/or the editor(s). MDPI and/or the editor(s) disclaim responsibility for any injury to people or property resulting from any ideas, methods, instructions or products referred to in the content.